



## **UWL REPOSITORY**

**repository.uwl.ac.uk**

Vibration-based Bayesian model updating of civil engineering structures  
applying Gaussian process metamodel

Moravej, Hossein, Chan, Tommy, Nguyen, Khac Duy and Jesus, Andre ORCID logoORCID:  
<https://orcid.org/0000-0002-5194-3469> (2019) Vibration-based Bayesian model updating of civil  
engineering structures applying Gaussian process metamodel. *Advances in Structural Engineering*,  
22 (16). pp. 3487-3502. ISSN 1369-4332

<http://dx.doi.org/10.1177/1369433219858723>

This is the Accepted Version of the final output.

**UWL repository link:** <https://repository.uwl.ac.uk/id/eprint/6130/>

**Alternative formats:** If you require this document in an alternative format, please contact:  
[open.research@uwl.ac.uk](mailto:open.research@uwl.ac.uk)

### **Copyright:**

Copyright and moral rights for the publications made accessible in the public portal are retained by the authors and/or other copyright owners and it is a condition of accessing publications that users recognise and abide by the legal requirements associated with these rights.

**Take down policy:** If you believe that this document breaches copyright, please contact us at [open.research@uwl.ac.uk](mailto:open.research@uwl.ac.uk) providing details, and we will remove access to the work immediately and investigate your claim.

### **Rights Retention Statement:**



## Vibration-based Bayesian model updating of civil engineering structures applying Gaussian process metamodel

Journal:	<i>Advances in Structural Engineering</i>
Manuscript ID	ASE-18-0610.R2
Manuscript Type:	Special Issue for Prof JM Ko
Date Submitted by the Author:	19-May-2019
Complete List of Authors:	Moravej, Hossein; Queensland University of Technology Faculty of Science and Engineering, Civil Engineering & Built Environment Chan, Tommy Nguyen, Khac Duy; Queensland University of Technology Faculty of Science and Engineering, Civil Engineering & Built Environment Jesus, Andre; University of West London, School of Computing and Engineering
Keywords:	Finite Element Model Updating, Bayesian framework, Gaussian process, Structural Health Monitoring, Box girder bridge, Vibration analysis
Abstract:	<p>Structural health monitoring plays a significant role in providing information regarding the performance of structures throughout their life spans. However, information that is directly extracted from monitored data is usually susceptible to uncertainties and not reliable enough to be used for structural investigations. Finite element model updating (FEMU) is an accredited framework that reliably identifies structural behavior. Recently, the modular Bayesian approach (MBA) has emerged as a probabilistic technique in calibrating the finite element model (FEM) of structures and comprehensively addressing uncertainties. However, few studies have investigated its performance on real structures. In this paper, MBA is applied to calibrate the FEM of a lab-scaled concrete box girder bridge. This study is the first to use the MBA to update the initial FEM of a real structure for two states—undamaged and damaged conditions—in which the damaged state represents changes in structural parameters as a result of aging or overloading. The application of the MBA in the two states provides an opportunity to examine the performance of the approach with observed evidence. A discrepancy function is used to identify the deviation between the outputs of the experimental and numerical models. To alleviate computational burden, the numerical model and the model discrepancy function are replaced by Gaussian processes. Results indicate a significant reduction in the stiffness of concrete in the damaged state, which is identical to cracks observed on the body of the structure. The discrepancy function reaches satisfying ranges in both states, which implies that the properties of the structure are predicted accurately. Consequently, the proposed methodology contributes to a more reliable judgment about structural safety.</p>

1  
2  
3  
4  
5  
6  
7  
8  
9  
10  
11  
12  
13  
14  
15  
16  
17  
18  
19  
20  
21  
22  
23  
24  
25  
26  
27  
28  
29  
30  
31  
32  
33  
34  
35  
36  
37  
38  
39  
40  
41  
42  
43  
44  
45  
46  
47  
48  
49  
50  
51  
52  
53  
54  
55  
56  
57  
58  
59  
60



# Vibration-based Bayesian model updating of civil engineering structures applying Gaussian process metamodel

Hossein Moravej, Tommy Chan, Khac-Duy Nguyen and

Andre Jesus

## Abstract

Structural health monitoring plays a significant role in providing information regarding the performance of structures throughout their life spans. However, information that is directly extracted from monitored data is usually susceptible to uncertainties and not reliable enough to be used for structural investigations. Finite element model updating (FEMU) is an accredited framework that reliably identifies structural behavior. Recently, the modular Bayesian approach (MBA) has emerged as a probabilistic technique in calibrating the finite element model (FEM) of structures and comprehensively addressing uncertainties. However, few studies have investigated its performance on real structures. In this paper, MBA is applied to calibrate the FEM of a lab-scaled concrete box girder bridge. This

1  
2  
3  
4  
5  
6  
7  
8  
9  
10  
11  
12  
13  
14  
15  
16  
17  
18  
19  
20  
21  
22  
23  
24  
25  
26  
27  
28  
29  
30  
31  
32  
33  
34  
35  
36  
37  
38  
39  
40  
41  
42  
43  
44  
45  
46  
47  
48  
49  
50  
51  
52  
53  
54  
55  
56  
57  
58  
59  
60

1 study is the first to use the MBA to update the initial FEM of a real structure  
2 for two states—undamaged and damaged conditions—in which the  
3 damaged state represents changes in structural parameters as a result of  
4 aging or overloading. The application of the MBA in the two states provides  
5 an opportunity to examine the performance of the approach with observed  
6 evidence. A discrepancy function is used to identify the deviation between  
7 the outputs of the experimental and numerical models. To alleviate  
8 computational burden, the numerical model and the model discrepancy  
9 function are replaced by Gaussian processes. Results indicate a significant  
10 reduction in the stiffness of concrete in the damaged state, which is identical  
11 to cracks observed on the body of the structure. The discrepancy function  
12 reaches satisfying ranges in both states, which implies that the properties  
13 of the structure are predicted accurately. Consequently, the proposed  
14 methodology contributes to a more reliable judgment about structural  
15 safety.

## 17 **Keywords**

18 Finite Element Model Updating, Bayesian framework, Gaussian process,  
19 Structural Health Monitoring, Box girder bridge, Vibration analysis

1  
2  
3  
4  
5  
6  
7  
8  
9  
10  
11  
12  
13  
14  
15  
16  
17  
18  
19  
20  
21  
22  
23  
24  
25  
26  
27  
28  
29  
30  
31  
32  
33  
34  
35  
36  
37  
38  
39  
40  
41  
42  
43  
44  
45  
46  
47  
48  
49  
50  
51  
52  
53  
54  
55  
56  
57  
58  
59  
60

## 1 Introduction

2 Civil infrastructure plays a significant role in keeping urban systems operational, but  
3 any malfunctions in routine performance can result in major hazards and even threaten  
4 lives. Therefore, it is important to regularly investigate the safety of infrastructure.  
5 Many researchers such as Frangopol (2011) and Li et al. (2016) have acknowledged  
6 the importance of monitoring the behaviors of structures using information provided  
7 by structural health monitoring (SHM). An accredited approach to addressing the  
8 aforementioned objective is finite element model updating (FEMU), which aims to  
9 improve the accuracy of the finite element models (FEMs) of real structures and  
10 reduce the discrepancy between the output of FEMs and experimental measurements.  
11 The availability of reliable FEMs of structures is beneficial in terms of evaluation of  
12 structural performance, reliability analysis, load-carrying capacity assessment, and  
13 damage detection.  
14 However, FEMU faces significant barriers that prevent it from reaching its peak  
15 efficiency. For example, computational burden, especially in the case of complex  
16 structures, makes this technique cumbersome, and in some cases, the process of  
17 updating may lead to ill-conditioned optimization problems with limited practical  
18 applicability. Although some approaches have recently been introduced to improve  
19 computational efficiency, such as the response surface method (Shahidi and Pakzad,

1  
2  
3  
4  
5  
6  
7  
8  
9  
10  
11  
12  
13  
14  
15  
16  
17  
18  
19  
20  
21  
22  
23  
24  
25  
26  
27  
28  
29  
30  
31  
32  
33  
34  
35  
36  
37  
38  
39  
40  
41  
42  
43  
44  
45  
46  
47  
48  
49  
50  
51  
52  
53  
54  
55  
56  
57  
58  
59  
60

1 2013) and the substructure technique (Weng et al., 2012), this challenge still needs to  
2 be addressed.

3 Another challenge when updating a model relates to addressing different sources  
4 of uncertainties. To overcome this problem, probabilistic approaches that are more  
5 reliable than their deterministic counterparts have been introduced in the field of  
6 FEMU (Jesus et al., 2014; Jesus et al., 2018). Deterministic techniques, which  
7 consider fixed values regarding input parameters and response outputs, rarely  
8 provide a satisfactory correlation between the numerical model and real data  
9 because of inherent structural uncertainties (Friswell and Mottershead, 2013). In  
10 contrast, probabilistic approaches do not regard input parameters as fixed numbers  
11 to lock the updating process in those values; instead, they consider a realistic  
12 statistical distribution for each parameter. This consideration is more logical  
13 because it is impossible to confidently assert a certain value for one parameter using  
14 an updating process because of the existence of uncertainties. Therefore, in most  
15 cases, probabilistic approaches are more reliable. According to Kennedy and  
16 O'Hagan (2001a, 2001b), the main sources of uncertainty in model prediction are  
17 uncertainty in model parameters, modeling errors, and uncertainty resulting from  
18 observation errors. Uncertainty in model parameters relates to inputs to the  
19 computer model that are unknown and cannot be identified directly from physical  
20 experiments, such as the material properties of a damaged structure. Another source

1 of uncertainty—modeling error or model inadequacy—refers to any assumptions  
2 or simplifications made while developing FEMs, such as considering a material  
3 linear, isotropic, and homogenous. This source of uncertainty occurs even when all  
4 parameters are accurately identified. The observation error (i.e., experimental  
5 uncertainty) is usually present in physical experiments. This type of uncertainty  
6 denotes variations that may occur in the experimental measurement even when the  
7 test is repeated with the same settings.

8 Despite the significant effects of the abovementioned uncertainties, few studies  
9 have addressed all of these aspects. A number of probabilistic approaches have  
10 been developed in FEMU, including the fuzzy number-based method, Kalman  
11 Filter-based technique, model falsification diagnosis method, Markov process-  
12 based method and sampling method. Among all probabilistic FEMU techniques,  
13 Bayesian updating has been found to be one of the most applicable approaches for  
14 updating FEMs. Several attempts have been made to apply Bayesian updating, and  
15 Beck's method is eminent among them because it proposes a robust predictive  
16 approach (Beck and Katafygiotis, 1998; Beck and Au, 2002). The major weakness  
17 in the presentation of Bayesian methods in SHM practices is that uncertainty  
18 resulting from modeling errors is not properly considered. Only a few researchers  
19 have performed the Bayesian approach with consideration of this aspect (Higdon  
20 et al., 2008; Simoen et al., 2013). Higdon used a comprehensive modular Bayesian

1  
2  
3  
4  
5  
6  
7  
8  
9  
10  
11  
12  
13  
14  
15  
16  
17  
18  
19  
20  
21  
22  
23  
24  
25  
26  
27  
28  
29  
30  
31  
32  
33  
34  
35  
36  
37  
38  
39  
40  
41  
42  
43  
44  
45  
46  
47  
48  
49  
50  
51  
52  
53  
54  
55  
56  
57  
58  
59  
60

1 approach (MBA) that was formerly established by Kennedy and O'Hagan (2001a),  
2 but it was not generally successful in addressing identifiability. Identifiability  
3 represents the ability to achieve the true value of model parameters based on  
4 available data to illustrate a physical property such as Young's modulus (Arendt et  
5 al., 2012a). Arendt et al. (2012b) proposed an improvement to Kennedy and  
6 O'Hagan's original formulation using the MBA to overcome the identifiability  
7 problem by applying measured data with various responses. This method replaces  
8 an FEM with a Gaussian process (GP) model as a metamodel (Kennedy and  
9 O'Hagan, 2001a). It has been found that the method significantly reduces  
10 computational effort—especially in cases of complex structures (Lophaven et al.,  
11 2002; Jesus et al., 2017; Conde et al., 2019; Jesus et al., 2019). The GP model  
12 for interpolation that considers uncertainties is found to be effective, even if data  
13 are limited. This formulation is preferable to former studies in model updating  
14 because it comprises the main sources of uncertainties and consequently reaches  
15 more realistic outcomes.

16 Based on the thriving interest in the MBA, this study validates its practical  
17 performance in FEMU by means of measured vibration data. The study investigates  
18 the applicability of the algorithm to a lab-scaled reinforced concrete box girder  
19 bridge (BGB), which represents a typical hollow core bridge deck in Australia. The  
20 MBA is applied in two states—undamaged and damaged—to calibrate multiple

1 parameters of the FEM. The performance of the approach is examined according  
2 to the observed evidence of the undamaged condition with initial minor cracks and  
3 the damaged condition with imposed cracks. The damaged state represents changes  
4 in structural parameters as a result of aging or overloading. Accordingly, this study  
5 aims to identify changes in the structural parameters and provide a reliable updated  
6 model for each state. The structural identification provided through the applied  
7 framework will not only provide a better understanding of structural performance,  
8 but will also contribute to providing suitable guidelines for decision-making  
9 regarding maintenance actions.

10

## 11 **Model Updating Methodology**

12 This section describes the model updating approach used in this study. The first  
13 subsection explains the connecting equation between the observations and the outputs  
14 of the numerical model. The second subsection briefly presents the GP, and the last  
15 subsection outlines the framework.

16

17

18

1  
2  
3  
4  
5  
6  
7  
8  
9 **1 Observation and numerical model relationship**

10  
11  
12 2 We assume that a real and unobservable process  $f$  has  $n$  observations of  $q$  responses

13  
14 3  $\mathbf{Y}^e$  from the measured data, where the superscript “e” is the experimental model.

15  
16  
17 4 The relationship between  $f$  and  $\mathbf{Y}^e$  can be denoted as equation (1):

18  
19  
20  
21  
22  
23 6 
$$\mathbf{Y}^e = \mathbf{f} + \boldsymbol{\varepsilon} \quad (1)$$

24  
25  
26  
27  
28 8 where  $\boldsymbol{\varepsilon} = [\varepsilon_1, \dots, \varepsilon_n]^T$  is the observation error, which is supposed to work as a

29  
30 9 Gaussian distribution with a mean of 0 and variance of  $\Lambda \in \mathbb{R}$ . Alternatively, the

31  
32  
33 10 real process  $f$  can be interpreted as equation (2) to comprise the numerical model:

34  
35  
36  
37  
38  
39 12 
$$\mathbf{f} = \mathbf{Y}^m(\boldsymbol{\theta}^*) + \boldsymbol{\delta} \quad (2)$$

40  
41  
42  
43  
44 14 where  $\boldsymbol{\delta}$  is a discrepancy function that represents the difference between the

45  
46 15 numerical model and the real process.  $\mathbf{Y}^m(\boldsymbol{\theta}^*)$  is the numerical model’s output and

47  
48 16  $\boldsymbol{\theta}^*$  is an  $r$ -dimensional vector of the true structural parameters. This equation is an

49  
50  
51 17 idealized form of the final model (i.e., the model after successful calibration), while

52  
53  
54 18 the model parameters  $\boldsymbol{\theta}$  take the values  $\boldsymbol{\theta}^*$ . Significantly, the discrepancy function

1  
2  
3  
4  
5  
6  
7  
8  
9 does not depend on the model's output and is an unknown in addition to the  
10 structural parameters. Equation (2) is then substituted into equation (1) to obtain  
11  
12  
13  
14 equation (3):  
15  
16

$$17 \quad \mathbf{Y}^e = \mathbf{Y}^m(\theta^*) + \boldsymbol{\delta} + \boldsymbol{\varepsilon} \quad (3)$$

18  
19  
20  
21  
22  
23  
24 Equation (3) is a comprehensive equation of the model updating process. It denotes  
25  
26  
27  
28  
29  
30  
31  
32  
33  
34  
35  
36  
37  
38  
39  
40  
41  
42  
43  
44  
45  
46  
47  
48  
49  
50  
51  
52  
53  
54  
55  
56  
57  
58  
59  
60  
the output of the processes within the domain of a calibrated status  $\theta = \theta^*$ , which  
implies the best fit compared with the observed data.

10 In the next step, the numerical model and the discrepancy function are substituted  
11  
12  
13  
14  
15  
16  
17  
18  
19  
20  
21  
22  
23  
24  
25  
26  
27  
28  
29  
30  
31  
32  
33  
34  
35  
36  
37  
38  
39  
40  
41  
42  
43  
44  
45  
46  
47  
48  
49  
50  
51  
52  
53  
54  
55  
56  
57  
58  
59  
60  
with two multiple-response Gaussian processes (MRGPs) whose hyperparameters  
must be found. These hyperparameters describe the MRGPs and illustrate the  
approximation of their associated uncertainties such as variability of the numerical  
model, modeling discrepancies, and observation errors.

### 16 *Gaussian Process*

17 Gaussian processes (GP) modeling is an interpolation approach that considers  
18  
19  
20  
21  
22  
23  
24  
25  
26  
27  
28  
29  
30  
31  
32  
33  
34  
35  
36  
37  
38  
39  
40  
41  
42  
43  
44  
45  
46  
47  
48  
49  
50  
51  
52  
53  
54  
55  
56  
57  
58  
59  
60  
uncertainty highly efficient even when data are limited (Kennedy and O'Hagan,  
2001a; Rasmussen et al., 2006). By applying interpolations and extrapolations, this

1  
2  
3  
4  
5  
6  
7  
8  
9  
10  
11  
12  
13  
14  
15  
16  
17  
18  
19  
20  
21  
22  
23  
24  
25  
26  
27  
28  
29  
30  
31  
32  
33  
34  
35  
36  
37  
38  
39  
40  
41  
42  
43  
44  
45  
46  
47  
48  
49  
50  
51  
52  
53  
54  
55  
56  
57  
58  
59  
60

1 approach offers a predicted GP that is fitted on all observation points. In this study,  
2 an MRGP is applied by assuming that the metamodel of model  $\mathbf{Y}$  is a single  
3 realization of a spatial random process with a prior mean function and covariance  
4 function (O'Hagan, 2006; Rasmussen et al., 2006). Regarding approximation of the  
5 metamodel, it is assumed that a dataset of  $\mathbf{Y}$  with a size of  $g$  and  $N$  observations  
6 should be available as input. Dimension  $g$  represents the number of responses ( $Y_1,$   
7  $Y_2, \dots, Y_g$ ). To generate the MRGP, the mean function is required to be obtained,  
8 which exists at every design input point without uncertainty. In the spaces located  
9 between or outside the design input points, the MRGP will produce either a possible  
10 interpolation or extrapolation from the existing data points.

11 In the MRGP, the prior mean function is supposed to be a member of a hierarchical  
12 structure of linear functions. It can be generalized as the form  $\mathbf{M}=\mathbf{H}\boldsymbol{\beta}$ . Herein,  
13 matrix  $\mathbf{H}$  comprises  $N$  polynomial constant regression functions and the matrix of  
14 regression coefficient  $\boldsymbol{\beta}$  for each term included in matrix  $\mathbf{H}$  and each fitted response  
15 in  $\mathbf{Y}$ . That is,  $\mathbf{H}$  is a row vector of regression functions and  $\boldsymbol{\beta}$  is a column vector of  
16 regression functions.

17 The prior covariance function of the MRGP for the model and discrepancy function  
18 can be formulated as equation (4):

19

$$\mathbf{V} = \Sigma^2 \otimes \mathbf{R} \quad (4)$$

where  $\mathbf{V}$  is covariance function,  $\Sigma^2 \in \mathbb{R}^{g \times g}$  is a non-temporal variance matrix, and  $\mathbf{R} \in \mathbb{R}^{N \times N}$  is a temporal correlation matrix, and  $\otimes$  is the Kronecker product operation on the two matrices. This equation can be interpreted as the separation of a variance between the  $g$  responses (which are being approximated) and a correlation between the  $N$  times histories. Each entry of Matrix  $\mathbf{R}$  contains a correlation function that needs to be approximated. This assumption is applicable to the correlation function of the numerical model. In addition, because the FEM is linear, a linear correlation function is assumed for the correlation function in this study, as shown in equation (5). This model fits properly to the data and is numerically stable (Lophaven et al., 2002).

$$\mathbf{R}(\omega, \theta, \theta') = \prod_{j=1}^r \max \{0, 1 - \omega_j |\theta_j - \theta'_j|\} \quad (5)$$

In equation (5),  $\omega_j$  ( $j=1, \dots, r$ ) is the roughness parameter and represents how roughly the responses change from point  $\theta$  to point  $\theta'$  for each of the structural parameters of interest.

1 In contrast, the correlation matrix for the discrepancy function is simply assumed  
 2 as an identity matrix as  $\mathbf{R}=\mathbf{I}$ . This assumption implies that the final predicted  
 3 responses have no temporal correlation. This is reasonable for natural frequencies  
 4 obtained from a laboratory model because they vary randomly without any definite  
 5 relations. The final hyperparameter that needs to be estimated to conclude the  
 6 description of the MRGP is  $\Lambda$  as the  $N \times 1$  variance vector of the observation error  
 7  $\varepsilon$ , which can simply be added to equation (4) to reach equation (6).

$$\mathbf{V} = \Sigma^2 \otimes \mathbf{R} + \Lambda \quad (6)$$

11 After providing a certain amount of data  $\mathbf{Y}$ , the MRGP is provided (supposing a non-  
 12 informative prior for  $\boldsymbol{\beta}$  and given  $\omega$  and  $\Sigma$ ). The posterior distribution of the response  
 13 is given by equation (7):

$$y \mid \Sigma, \omega, \Lambda, \mathbf{Y} \sim N(m^*, \Sigma \otimes \mathbf{y}^*) \quad (7)$$

17 with

$$m^* = h\hat{\boldsymbol{\beta}} + \mathbf{y}^T \Gamma^{-1} (\mathbf{Y} - \mathbf{H} \hat{\boldsymbol{\beta}}) \quad (8)$$

1

$$\mathbf{y}^* = \mathbf{y} - \mathbf{y}^T \mathbf{\Gamma}^{-1} \mathbf{y} + [\mathbf{h}^T - \mathbf{H}^T \mathbf{\Gamma}^{-1} \mathbf{y}]^T [\mathbf{H}^T \mathbf{\Gamma}^{-1} \mathbf{H}]^{-1} [\mathbf{h}^T - \mathbf{H}^T \mathbf{\Gamma}^{-1} \mathbf{y}] \quad (9)$$

2 where  $\mathbf{y}$  represents the MRGP,  $\mathbf{h}$  is the hierarchical structure of regression  
 3 functions.  $\mathbf{y}$  is defined as a relational correlation matrix, which maps the correlation  
 4 between the indices of points of available dataset and the indices of points supposed  
 5 to be predicted (Conti et al., 2009). The used correlation function is the same as  
 6 equation (5).  $\hat{\boldsymbol{\beta}}$  stands for the estimated matrix of  $\boldsymbol{\beta}$  and is given by calculating  
 7 equation (10):  
 8

9

$$\mathbf{H}^T \mathbf{R}^{-1} \mathbf{H} \hat{\boldsymbol{\beta}} = \mathbf{H}^T \mathbf{R}^{-1} \mathbf{Y} \quad (10)$$

11

12 which refers to the linear regression solution of the best linear unbiased predictor.  
 13  $\mathbf{\Gamma}$  is an  $N \times N$  correlation matrix that contains the linear functions. The MRGP in  
 14 equation (7) can be defined by estimating the hyperparameters  $\omega$ ,  $\boldsymbol{\beta}$ ,  $\Sigma$ , and  $\Lambda$ .  
 15 Characterization of the hyperparameters can be conducted using a Bayesian  
 16 approach, which would address all of the mentioned uncertainties and identify all  
 17 of the hyperparameters at the same time. However, this approach is not efficient  
 18 because it comprises a huge computational process (Liu et al., 2009). Therefore,  
 19 for better computational efficiency, the hyperparameters are calculated with the

1  
2  
3  
4  
5  
6  
7  
8  
9 1 maximum likelihood estimations (MLEs). A more comprehensive description of  
10  
11 2 the GP method can be found in Arendt et al. (2012a).

### 13 3 *Modular Bayesian approach (MBA)*

14  
15  
16  
17  
18 4 The MBA separates the updating process into four steps. The hyperparameters of  
19  
20 5 the MRGP are approximated separately and consecutively, as shown in Figure 5 in  
21  
22 6 the study by Arendt et al. (2012a). In the MBA, the hyperparameters continue to be  
23  
24 7 estimated until the first order of uncertainties is found, and then they are fixed. It is  
25  
26 8 worth noting that setting up the hyperparameters at fixed estimations decreases the  
27  
28 9 degree of approximation of the uncertainties. In addition, the “second-order”  
29  
30 10 resolution of the uncertainties is ignored to alleviate the computational burden and  
31  
32 11 make it faster than fully considering the uncertainties in the Bayesian framework.  
33  
34 12 This act of estimating and fixing the hyperparameters is performed sequentially  
35  
36 13 when progressing from module 1 to module 2 and from module 2 to module 3.

37  
38  
39  
40  
41  
42 14 The first module basically substitutes the computer model to an MRGP model and  
43  
44 15 estimates its hyperparameters based on only the simulation data. In this module,  
45  
46 16 the simulation is run in finite element modeling software (e.g., Abaqus) to obtain  
47  
48 17 the simulated responses by randomly changing the input parameters using Latin  
49  
50 18 hypercube sampling (LHS). For the experimental validation in this study, 120 and  
51  
52 19 80 runs were conducted in the undamaged and damaged states, respectively, to  
53  
54  
55  
56  
57  
58  
59  
60

1 provide a dataset. The estimation can be carried out using numerical optimization  
2 methods by fitting a likelihood between the MRGP and the available simulation  
3 data. In this study, a genetic algorithm (GA) routine was applied in MATLAB. For  
4 the GA setup, an initial population of size 40 is generated in the [0; 1] range, a  
5 Gaussian mutation function with a scale of 1 (i.e., initial standard deviation of 1)  
6 and a standard deviation shrink of 1 is chosen, and a scattered crossover function  
7 applied to a portion of 0.8 of the population at each generation is defined.  
8 Convergence criteria are set as either a maximum number of 100 generations or  
9 until an average change in the fitness value of  $1 \times 10^{-6}$  is reached.

10 In module 2, the discrepancy function is estimated by fitting another MRGP model  
11 according to the measured data from the experiment, the simulation data, and the  
12 prior distribution of the calibration parameters. The GA is used to approximate the  
13 discrepancy function by estimating the hyperparameters of the GP. This task is  
14 carried out by an MLE, which indicates that the fitness function of the GA is a  
15 likelihood function. It should be mentioned that either the MBA or the full Bayesian  
16 approach can estimate the hyperparameters of the abovementioned MRGP models  
17 through MLE and Bayesian posterior distributions, respectively. As discussed in  
18 the previous section, the MBA is used in this study because Bayesian posterior  
19 distributions can be computationally inefficient. In addition, according to Bayarri

1  
2  
3  
4  
5  
6  
7  
8  
9  
10  
11  
12  
13  
14  
15  
16  
17  
18  
19  
20  
21  
22  
23  
24  
25  
26  
27  
28  
29  
30  
31  
32  
33  
34  
35  
36  
37  
38  
39  
40  
41  
42  
43  
44  
45  
46  
47  
48  
49  
50  
51  
52  
53  
54  
55  
56  
57  
58  
59  
60

1 et al. (2007), both approaches have similar results in predicting the discrepancy  
2 function and calibration parameters.

3 In module 3, Bayes' theorem is applied to approximate the posterior distribution of  
4 the updated parameters and its likelihood function containing the two MRGP  
5 models approximated in modules 1 and 2. Since multiple parameters are calibrated  
6 in this study, a Markov chain Monte Carlo method can be used to estimate the  
7 MBA. This choice implies that a target distribution must be used, and in this study,  
8 a multivariate normal distribution is chosen (Arendt et al., 2012b).

9 In module 4, the experimental responses are calculated by applying the measured  
10 data and the estimated hyperparameters obtained from modules 1 and 2. After the  
11 simulated and measured data are collected in modules 1 and 2 and the calibrated  
12 parameters are estimated in module 3, the posterior distribution response of the  
13 updated model together with the updated discrepancy function can be obtained. For  
14 the prediction of the responses, 40 measured data points for the undamaged state  
15 and 60 data points for the damaged state are randomly distributed along the  
16 simulated data points. It is worth noting that simulated data have been provided by  
17 applying the LHS approach as described in the first module. In addition, it is  
18 assumed that the measured responses are independent of time, temperature  
19 variation, and other operational effects.

1  
2  
3  
4  
5  
6  
7  
8  
9  
10  
11  
12  
13  
14  
15  
16  
17  
18  
19  
20  
21  
22  
23  
24  
25  
26  
27  
28  
29  
30  
31  
32  
33  
34  
35  
36  
37  
38  
39  
40  
41  
42  
43  
44  
45  
46  
47  
48  
49  
50  
51  
52  
53  
54  
55  
56  
57  
58  
59  
601  
2  
3  
4  
5  
6  
7  
8  
9  
10  
11  
12  
13  
14  
15  
16  
17  
18  
19  
20  
21  
22  
23  
24  
25  
26  
27  
28  
29  
30  
31  
32  
33  
34  
35  
36  
37  
38  
39  
40  
41  
42  
43  
44  
45  
46  
47  
48  
49  
50  
51  
52  
53  
54  
55  
56  
57  
58  
59  
60

## **Finite element model updating for a box girder bridge**

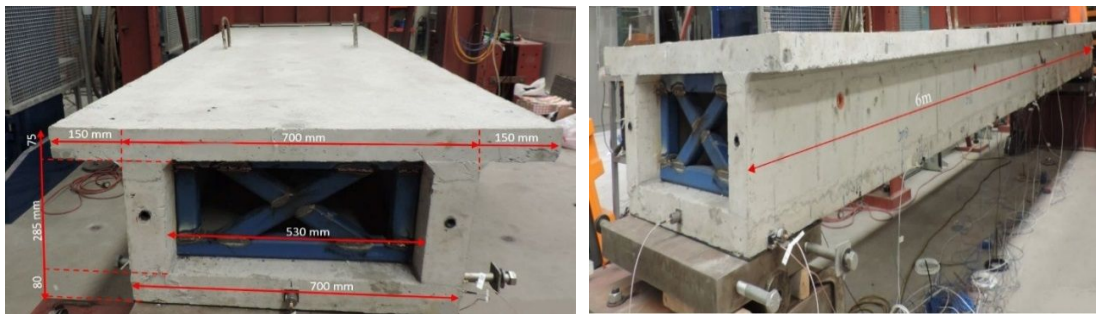
The first subsection presents details of the BGB and two different states (i.e., undamaged and damaged) of the structure. Details of an FEM and experimental modal analysis as two counterparts in model updating are provided in the second and third subsections, respectively. The fourth subsection highlights sensitivity analysis as a tool to select appropriate parameters and responses in FEMU.

### ***Two states of box girder bridge***

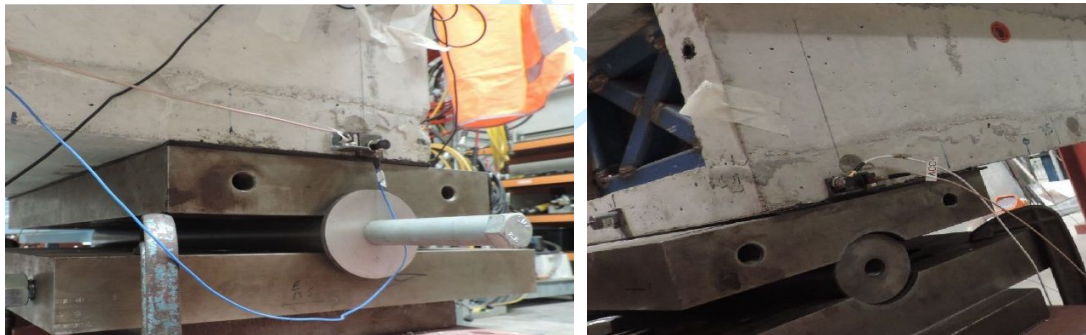
A downscaled reinforced concrete BGB, which was constructed in the civil engineering laboratory at the Queensland University of Technology, is investigated in this study. This structure represents a typical in-service hollow core bridge deck in Australia. The length of the BGB is 6 m, and it was cast in three separate parts as the bottom slab, the webs, and the top slab. Detailed dimensions of the structure are shown in Figure 1 (a). Further information about the casting steps can be found in Pathirage (2017). The BGB was placed on two simple supports as a pin at one end and a roller at the other end, as shown in Figure 1 (b). This platform refers to

1 the undamaged state (first state), despite the existence of some minor cracks  
 2 beneath the soffit slab.

3



4 (a)



5 (b)

6 **Figure 1.** The BGB details: (a) BGB's dimensions and (b) Boundary conditions in BGB as Roller (left) and  
 7 Pin (right).

8

9 In the second state (damaged state), a point load and then a cyclic load were applied  
 10 at the midspan of the BGB. These impacts resulted in some significant cracks on  
 11  
 12

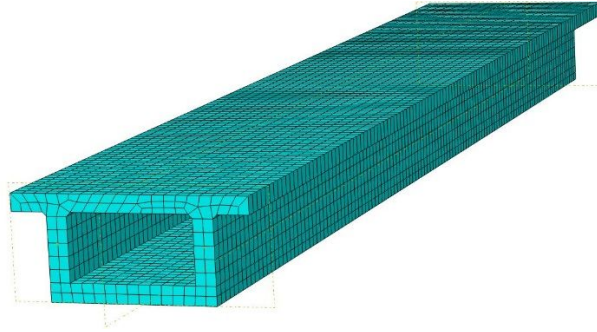
1 the soffit slab and the webs of the BGB. Eight significant cracks were observed,  
2 each of which ran through the whole width of the bottom slab and propagated to  
3 the webs. Figure 2 shows some observed cracks on the body of the structure.



6  
7 **Figure 2.** Detected cracks on body of the BGB in damaged state.

### 9 *Numerical model*

10 Given the lack of available information about the structural parameters of the BGB,  
11 such as material properties and boundary conditions, nominal values of the  
12 parameters were assumed from the designing details and were used to create a  
13 numerical model of the BGB. The initial BGB's FEM was built in the Abaqus  
14 software package, as shown in Figure 3 (Abaqus, 2017).



1  
2  
3  
4  
5  
6  
7  
8  
9  
10  
11  
12  
13  
14  
15  
16  
17  
18  
19  
20  
21  
22  
23  
24  
25  
26  
27  
28  
29  
30  
31  
32  
33  
34  
35  
36  
37  
38  
39  
40  
41  
42  
43  
44  
45  
46  
47  
48  
49  
50  
51  
52  
53  
54  
55  
56  
57  
58  
59  
60

**Figure 3.** FEM of BGB built in ABAQUS 2017.

From the Abaqus element library, a C3D8R solid element and a T3D2 truss element were assigned to the concrete and reinforcement elements, respectively. Regarding material properties, according to the design details, Young's modulus ( $E$ ) is assumed as 200 (GPa) for reinforcement and 32 (GPa) for concrete. Further, mass density ( $\rho$ ) is assumed as 7,850 kg/m<sup>3</sup> for reinforcement and 2,400 kg/m<sup>3</sup> for concrete. In addition, the boundary conditions were considered fixed in vertical displacement for both supports. In this study, a convergence assessment for mesh size selection was performed by applying a load-displacement control. Herein, load against midspan deflection was examined for different mesh sizes. A mesh size of 50 mm was determined to be fit enough by considering the experimental displacement at the mid-zone in failure mode. More details of the analysis can be found in Jamali et al. (2018). In this study, four natural frequencies of the FEM—first vertical bending, second vertical bending, first lateral bending, and third vertical bending modes—were selected

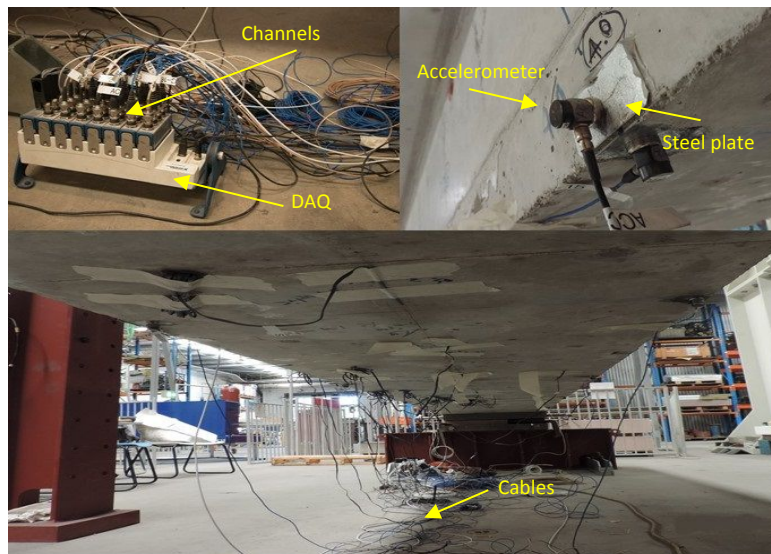
1 and used to update the FEM because similar mode shapes and natural frequencies were  
2 extracted from the measured data.

#### 3 4 *Modal data analysis*

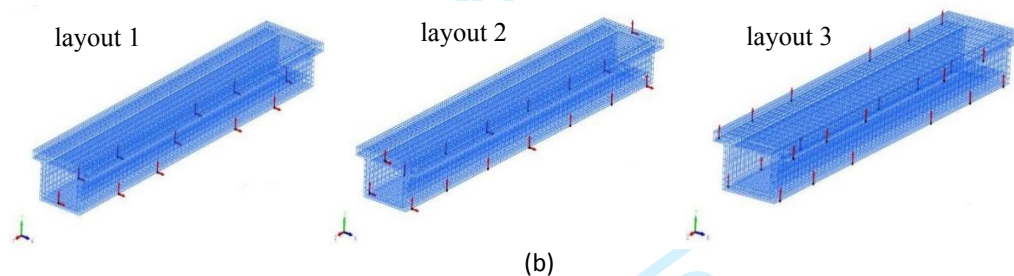
5 During the casting process of the BGB, several small steel plates were attached to  
6 the BGB's surface to facilitate sensor installation. The sensory system used in this  
7 study is shown in Figure 4 (a). Regarding the selection of the right sensor layout,  
8 different aspects were noticed in relation to the number and type of available  
9 sensors, the excitation source, and the maximum number of channels in the data  
10 acquisition system. More details regarding the preparation of the experiment can  
11 be found in Jamali et al. (2016). The BGB was excited by applying multipoint  
12 random excitation with an impact hammer for each vibration test. Vibration  
13 responses were recorded using a data acquisition system. In this study, the vibration  
14 responses of the structure in both the undamaged and damaged states were  
15 measured and used in the FEMU process. Figure 4 (b) shows three examples of  
16 sensor layout arrangements that were applied in the modal analysis in this research.  
17 Each arrow in the figure represents a single sensor in the corresponding direction.

18

19



(a)

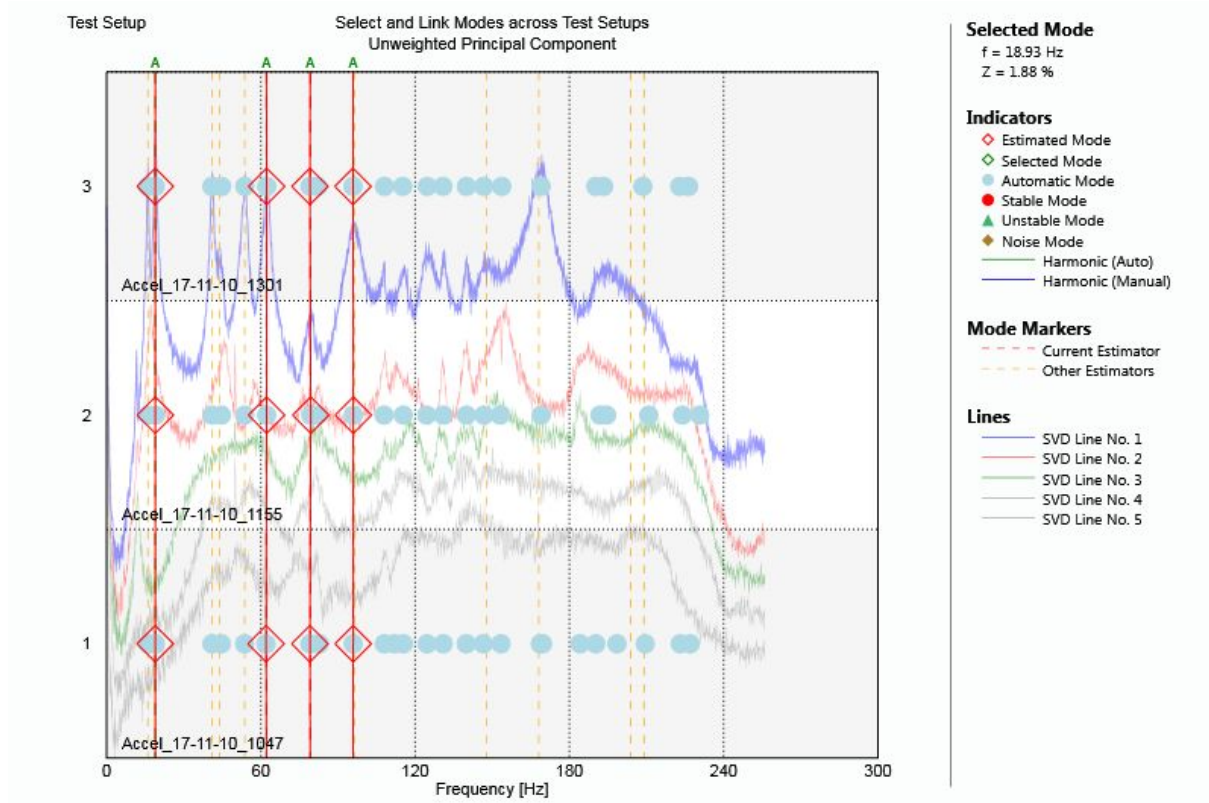


(b)

**Figure 4.** Structural response measurement: (a) Sensory system on the BGB and (b) Sensor layouts.

The measured acceleration responses were post-processed in the modal analysis step. In this regard, the stochastic subspace identification (SSI) method, which is embedded in the ARTeMIS Modal software package, was applied (ARTeMIS, 2011). An example of modal analysis for a dataset is illustrated in Figure 5.

1



2

3

Figure 5. Modal Analysis to capture experimental frequency in ARTeMIS.

4

5 Modal parameters for 40 datasets in the undamaged state and 60 datasets in the  
6 damaged state were analyzed. The test was conducted in a controlled environment  
7 in the laboratory, where ambient effects had little effect on the measured responses;  
8 therefore, the number of modal analyses in both states was sufficient. The detected  
9 natural frequencies were the first vertical bending, second vertical bending, first

1 lateral bending, and third vertical bending modes, similar to the FEM's results.  
 2 These modes were selected for the FEMU process because they could be detected  
 3 in both the undamaged and damaged states. The four measured mode shapes were  
 4 transferred into the FEMtools software package (Dynamic Design Solutions,  
 5 2012). The number of degrees of freedom (DOF) of an experimental model is often  
 6 smaller than that of the corresponding FEM as a result of a lack of available sensors  
 7 (Moravej et al., 2017). In this study, a coordinate expansion technique was applied  
 8 to increase the number of DOFs of the experimental model to the same number in  
 9 the FEM (Moravej et al., 2017). The values of the natural frequencies in both states  
 10 are shown in Table 1. In this table, the mode order refers to the ordering number of  
 11 the modes. The experimental and numerical mode shapes are illustrated in Figure  
 12 6.

14 **Table 1.** Frequency in the initial designed model and measured frequency in two states

Mode order	Freq as Designed (Hz)	Measured Freq (Undamaged)		Error (%)	Measured Freq (Damaged)		Error (%)
		Mean value (Hz)	STD		Mean value (Hz)	STD	
1	24.339	21.65	0.106	-12.42	18.78	0.082	-29.60
2	81.29	67.06	0.21	-21.22	63.06	0.174	-28.9
3	92.108	84.32	0.124	-9.24	80.73	0.14	-14.09
4	109.75	98.21	0.18	-11.75	95.74	1.023	-14.63

15

1  
2  
3  
4  
5  
6  
7  
8  
9  
10  
11  
12  
13  
14  
15  
16  
17  
18  
19  
20  
21  
22  
23  
24  
25  
26  
27  
28  
29  
30  
31  
32  
33  
34  
35  
36  
37  
38  
39  
40  
41  
42  
43  
44  
45  
46  
47  
48  
49  
50  
51  
52  
53  
54  
55  
56  
57  
58  
59  
60

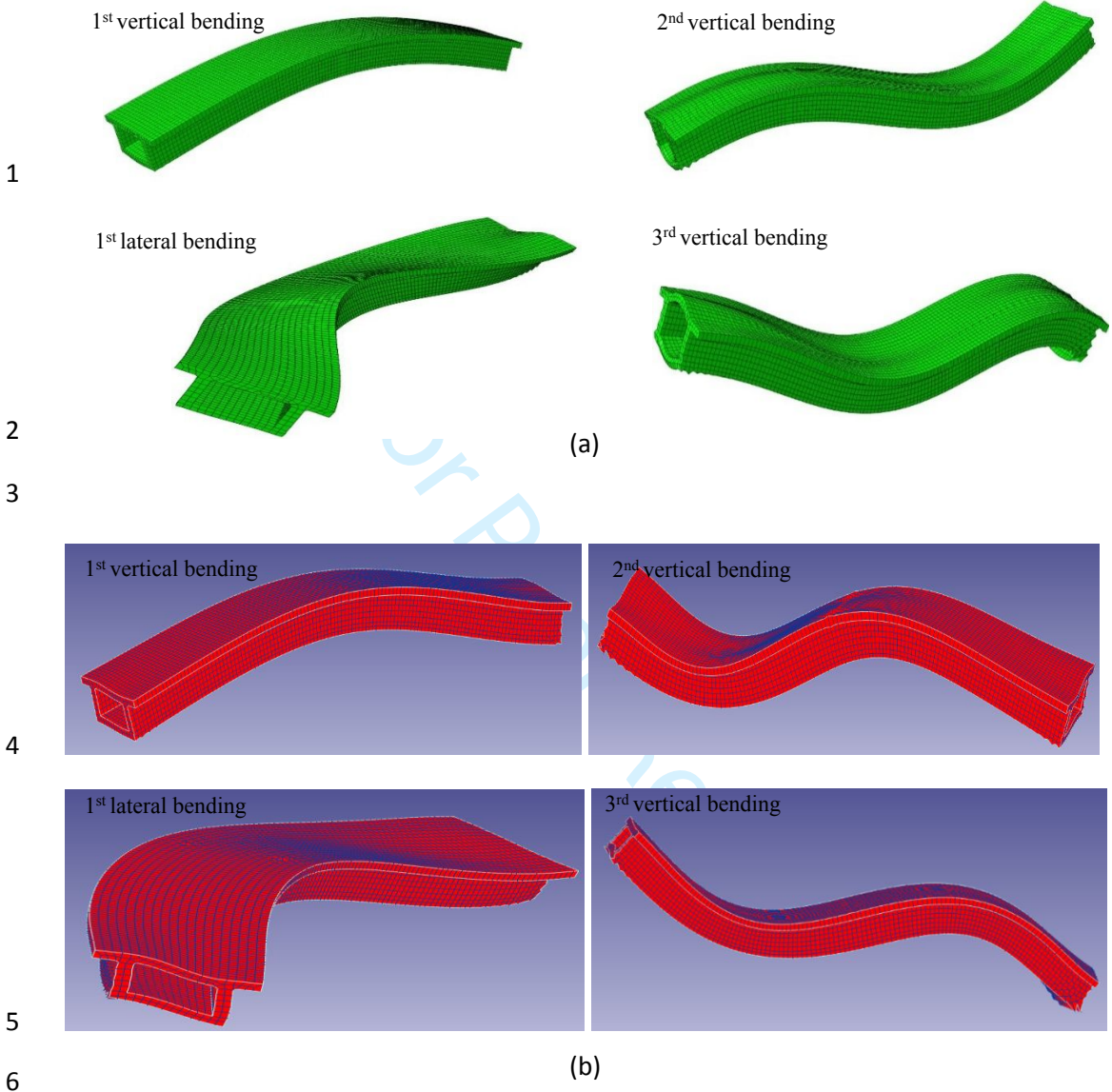


**Figure 6.** Four mode shapes: (a) Numerical model and (b) Measured model.

1  
2  
3  
4  
5  
6  
7  
8  
9  
10  
11  
12  
13  
14  
15  
16  
17  
18  
19  
20  
21  
22  
23  
24  
25  
26  
27  
28  
29  
30  
31  
32  
33  
34  
35  
36  
37  
38  
39  
40  
41  
42  
43  
44  
45  
46  
47  
48  
49  
50  
51  
52  
53  
54  
55  
56  
57  
58  
59  
60

## 1 *Sensitivity analysis*

2 A key step in most model updating approaches is the selection of appropriate  
3 parameters and responses in advance to initiate the updating process. Sensitivity  
4 analysis is a technique used to select the most sensitive parameters to the responses  
5 of a numerical model. This technique tends to analyse the effect of a very small  
6 perturbation of a parameter's value on a response by sketching the tangents on the  
7 response-parameter curve (Mottershead and Friswell, 2011). In this study,  
8 differential sensitivity analysis was applied to choose the most sensitive parameters  
9 to the selected responses using FEMtools (Dynamic Design Solutions, 2012). A  
10 differential sensitivity coefficient was calculated as the slope of the response  $T_i$  in  
11 relation to parameter  $B_j$  at a known state of the parameter. Once these differentials  
12 were calculated for all selected responses in relation to all selected parameters,  
13 sensitivity matrix  $\mathbf{S}$  was generated by equation (11).

$$15 \quad \mathbf{S} = S_{ij} = \frac{\delta T_i}{\delta B_j} \quad (11)$$

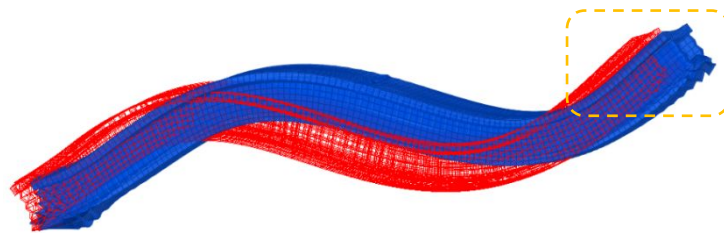
16 where:

17  $i: 1, \dots, n$   $T$ : Responses

18  $j: 1, \dots, n$   $B$ : Parameters

1 Each column of the sensitivity matrix corresponds with a parameter  $B_j$  and each  
2 row corresponds with a response  $T_i$ . Regarding the responses in this experiment,  
3 the four modal frequencies identified in the previous subsections were selected as  
4 sensitive responses. Details of the selected responses are shown in Table 1.

5 In the initial FEM, the simple supports were modelled as fixed in the vertical  
6 direction. However, by applying a correlation analysis between the mode shapes  
7 from the FEM and those from the experiment, it was observed that the roller in the  
8 experimental model was not fixed, as a bouncing was observed in the second  
9 vertical mode shape, as shown in Figure 7. Further, similar results were obtained  
10 for the third vertical bending mode shape. Therefore, a more accurate simulation of  
11 the boundary condition was used in this study to better represent the behavior of  
12 the structure.



13  
14 **Figure 7.** Correlation between FEM (Blue) and experimental (Red) in 2<sup>nd</sup> vertical mode shape.

1  
2  
3  
4  
5  
6  
7  
8  
9 1 For the updating process, the parameters related to concrete in three different parts  
10  
11 2 (i.e., bottom slab, webs, and top slab) were selected separately because the BGB  
12  
13 3 was cast in the three corresponding steps. Further, observed changes in the health  
14  
15 4 condition of the three parts were different after the damage was induced. Hence,  
16  
17 5 the parameter selection resulted in 10 parameters: (1) Young's modulus of concrete  
18  
19 6 (top), (2) Young's modulus of concrete (web), (3) Young's modulus of concrete  
20  
21 7 (bottom), (4) Young's modulus of reinforcement, (5) vertical spring stiffness  
22  
23 8 (roller), (6) vertical spring stiffness (pinned), (7) mass density of reinforcement, (8)  
24  
25 9 mass density of concrete (top), (9) mass density of concrete (web), and (10) mass  
26  
27 10 density of concrete (bottom). Results of the sensitivity analysis, as shown in Figure  
28  
29 11 8, provide a clearer picture of which parameters were sensitive to the selected  
30  
31 12 responses. The vertical axis in this figure refers to sensitivity magnitude. Based on  
32  
33 13 the sensitivity analysis, the selection resulted in the five most sensitive parameters:  
34  
35 14 Young's moduli of the bottom slab, the webs, and the top slab ( $E_{cBot}$ ,  $E_{cWeb}$ , and  
36  
37 15  $E_{cTop}$ ); and vertical spring stiffness coefficients of the two supports ( $K_{roller}$  and  $K_{pin}$ ).  
38  
39 16 Reducing the number of parameters of interest is essential to decrease the  
40  
41 17 computational cost.  
42  
43  
44  
45  
46  
47  
48  
49  
50  
51  
52  
53  
54  
55  
56  
57  
58  
59  
60

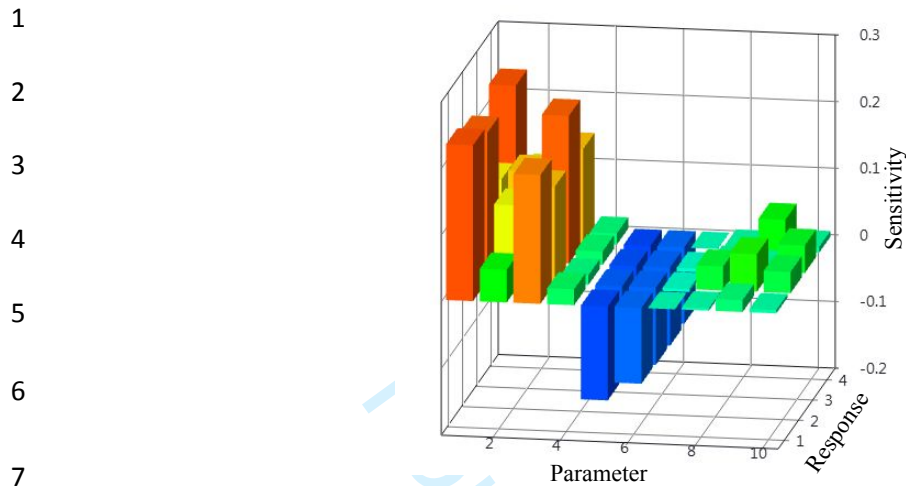


Figure 8. Sensitivity Analysis between selected parameters and responses.

## Result and discussion

The FEM of the BGB was updated for the two states—undamaged and damaged—by applying the MBA and using the four natural frequencies, mentioned in the previous section, as the responses. This section highlights the outcomes regarding the calibrated parameters and predicted responses in both states.

### *FEMU for undamaged state*

There was a lack of testing results from the casting stage, such as core sampling and tensile strength, to provide insights into prior distribution. Therefore, normal distributions were selected to represent all parameters' prior probability distribution

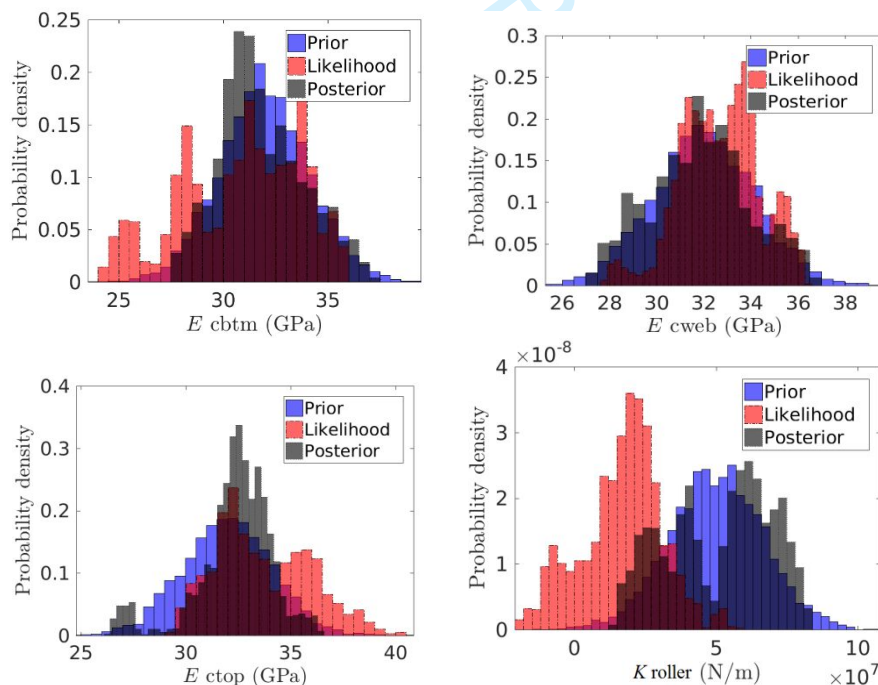
1 functions. This was in line with Mirza et al. (1980), Darmawan and Stewart (2007)  
 2 and recommendations from the code of practice AS-5104, as shown in Table 2.

3  
 4 **Table 2.** Parameter Prior Probability Distribution in Undamaged state

Parameter	Mean	Coefficient of Variation
( $E_{cTop}$ ) Young's modulus - Concrete - Top slab	32 GPa	7.13
( $E_{cWeb}$ ) Young's modulus - Concrete - Web	32 GPa	7.13
( $E_{cBot}$ ) Young's modulus - Concrete - Bottom slab	32 GPa	7.13
( $K_{Roller}$ ) Spring Stiffness Roller support	$5 \times 10^7$ N/m	$9 \times 10^{13}$
( $K_{Pin}$ ) Spring Stiffness Pinned support	$5 \times 10^7$ N/m	$9 \times 10^{13}$

5  
 6 In this study, the computational process was carried out using a computer equipped  
 7 with an Intel i7 quad-core processor with 3.4 GHz speed, 16 GB of RAM, and a  
 8 fast-access solid-state drive (SSD). For modules 1 and 2, hyperparameters were  
 9 obtained that characterize the estimation of the calibrated parameters and the  
 10 discrepancy function, and consequently represent the GPs. These hyperparameters  
 11 included a variance matrix  $\Sigma$ , a matrix of regression coefficient  $\beta$ , roughness  
 12 parameters  $\omega$ , and a noise variance matrix  $\Lambda$ , as explained in the methodology.  
 13 Results of the calibrated parameters after applying the MBA in the undamaged state  
 14 are illustrated in Figure 9 and Table 3. The posterior may require more data before  
 15 it faithfully represents the calibrated parameters; as a result, it did not present any

1 changes compared with the prior. It is worth noting that the likelihood identified  
 2 the calibrated parameters according to the measured data. As shown in Figure 9, in  
 3 the undamaged state, there were no considerable changes in Young's moduli of the  
 4 webs and the top slab in the likelihood against their priors. A significant change  
 5 was observed in the reduction in the bottom slab's Young's modulus ( $E_{cBot}$ ), which  
 6 was identical to the observed minor cracks beneath the BGB. Another noticeable  
 7 change was a reduction in vertical spring stiffness at the roller support, which infers  
 8 that the vertical fixity at the roller support was overestimated. This outcome is well  
 9 matched with the observed bouncing in the roller previously noticed in Figure 7.



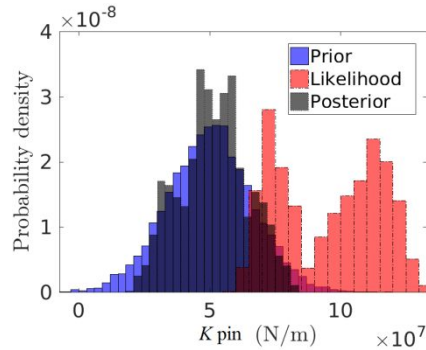


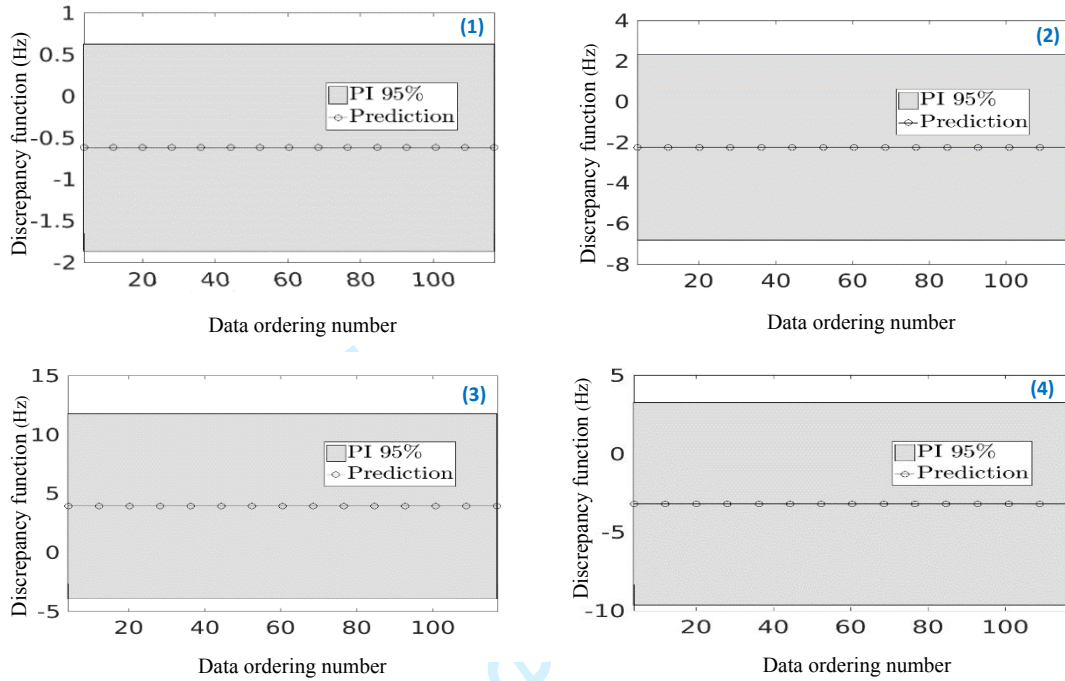
**Figure 9.** Prior, Max Likelihood and Posterior PDF for calibrated parameters in undamaged state.

**Table 3.** The Likelihood and Posterior distribution for calibrated parameters in undamaged state

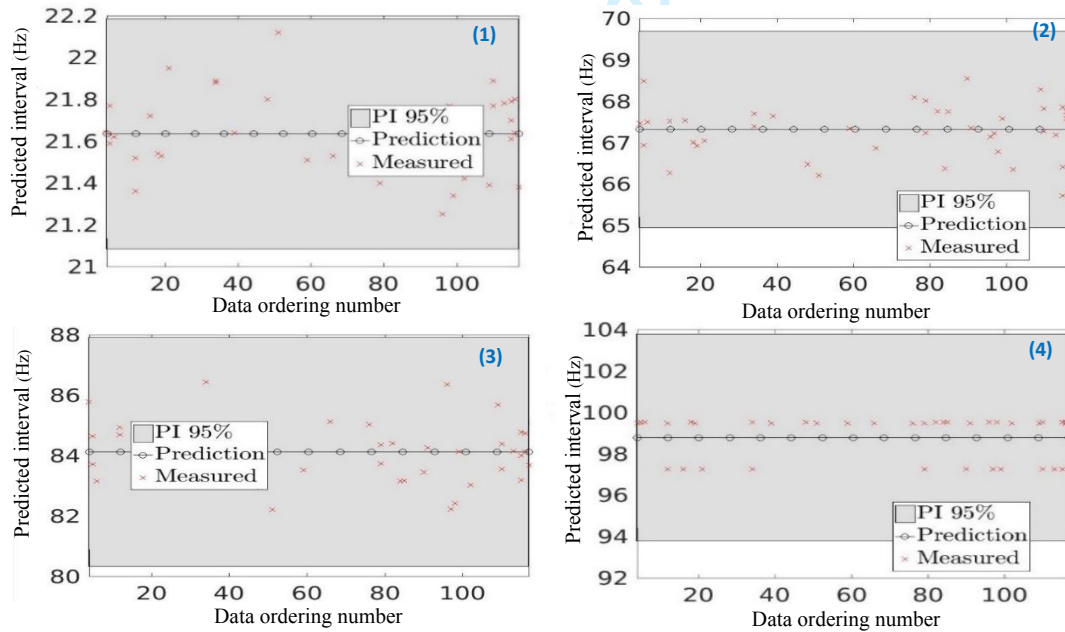
Part	Posterior		Likelihood	
	Mean	Coefficient of Variation	Mean	Coefficient of Variation
$E_{cBot}$	31.81 (GPa)	4.1	30.84 (GPa)	8.3
$E_{cWeb}$	31.83 (GPa)	4.5	32.69 (GPa)	2.9
$E_{cTop}$	32.34 (GPa)	3.4	33.67 (GPa)	5.2
$K_{Roller}$	$5.10 \times 10^7$ (N/m)	$3.32 \times 10^{14}$	$1.68 \times 10^7$ (N/m)	$2.02 \times 10^{14}$
$K_{Pin}$	$5.15 \times 10^7$ (N/m)	$1.66 \times 10^{14}$	$9.53 \times 10^7$ (N/m)	$3.82 \times 10^{14}$

The discrepancy functions for all four modes in the undamaged state are depicted in Figure 10 (a). In this figure, the horizontal axis represents the sample ordering numbers of the simulated data. The black line represents the predicted mean, and

1 the shaded region denotes a 95% prediction interval. As shown, the MBA predicted  
2 the measured responses accurately for all modes, with deviations of less than 6%.  
3 Figure 10 (b) depicts the measured responses together with the prediction intervals  
4 for all four modal frequencies. The measured data points obtained from the  
5 experimental tests, as shown by red spots in Figure 10 (b), are randomly distributed  
6 among the simulated data points. As shown, the measured data points are located  
7 in the 95% prediction interval and are very close to the mean values of the predicted  
8 responses. The predicted mean values almost coincide with those of the measured  
9 data points for all modes (see Table 1). However, it can be inferred from the  
10 predictions that the higher the mode order that is examined, the larger the scatter  
11 interval that is obtained.



(a) Discrepancy functions for frequency responses.



1  
2  
3  
4  
5  
6  
7  
8  
9  
10  
11  
12  
13  
14  
15  
16  
17  
18  
19  
20  
21  
22  
23  
24  
25  
26  
27  
28  
29  
30  
31  
32  
33  
34  
35  
36  
37  
38  
39  
40  
41  
42  
43  
44  
45  
46  
47  
48  
49  
50  
51  
52  
53  
54  
55  
56  
57  
58  
59  
60

1 (b) Predicted interval 95% confidence for numerical model and experimental data points.

2 **Figure 10.** The results of Discrepancy function and predicted response for numerical model in undamaged  
3 state for all four modal frequencies as: (1) 1<sup>st</sup> vertical bending frequency, (2) 2<sup>nd</sup> vertical bending  
4 frequency, (3) 1<sup>st</sup> lateral bending frequency & (4) 3<sup>rd</sup> vertical bending frequency.

### 5 *FEMU for damaged state*

7 The next step of model updating refers to the damaged state, where some significant  
8 cracks were observed on the bottom slab and the webs of the BGB. It is worth  
9 mentioning that the number of calibrated parameters was reduced to three (Young's  
10 moduli) because it was assumed that the applying impacts in the damaged state did  
11 not affect the boundary conditions. Results of the prior, likelihood, and posterior  
12 distributions of the calibrated parameters are illustrated in Figure 11 and Table 4.

13

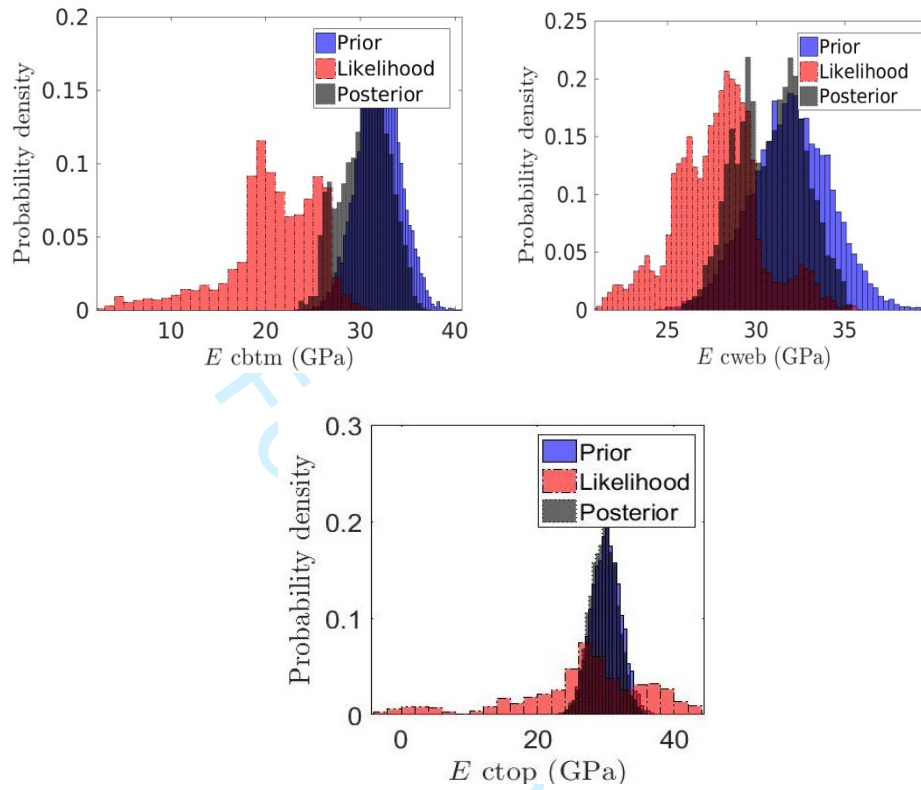


**Figure 11.** Prior, Max Likelihood and Posterior PDF for calibrated parameters in damaged state.

**Table 4.** The Likelihood and Posterior distribution for calibrated parameters in damaged state

Part	Posterior		Likelihood	
	mean	Coefficient of Variation	mean	Coefficient of Variation
$E_{cBot}$	30.45 (GPa)	6.45	20.63 (GPa)	25.59
$E_{cWeb}$	30.82 (GPa)	3.58	27.82 (GPa)	5.99
$E_{cTop}$	32.54 (GPa)	2.26	30.54 (GPa)	35.45

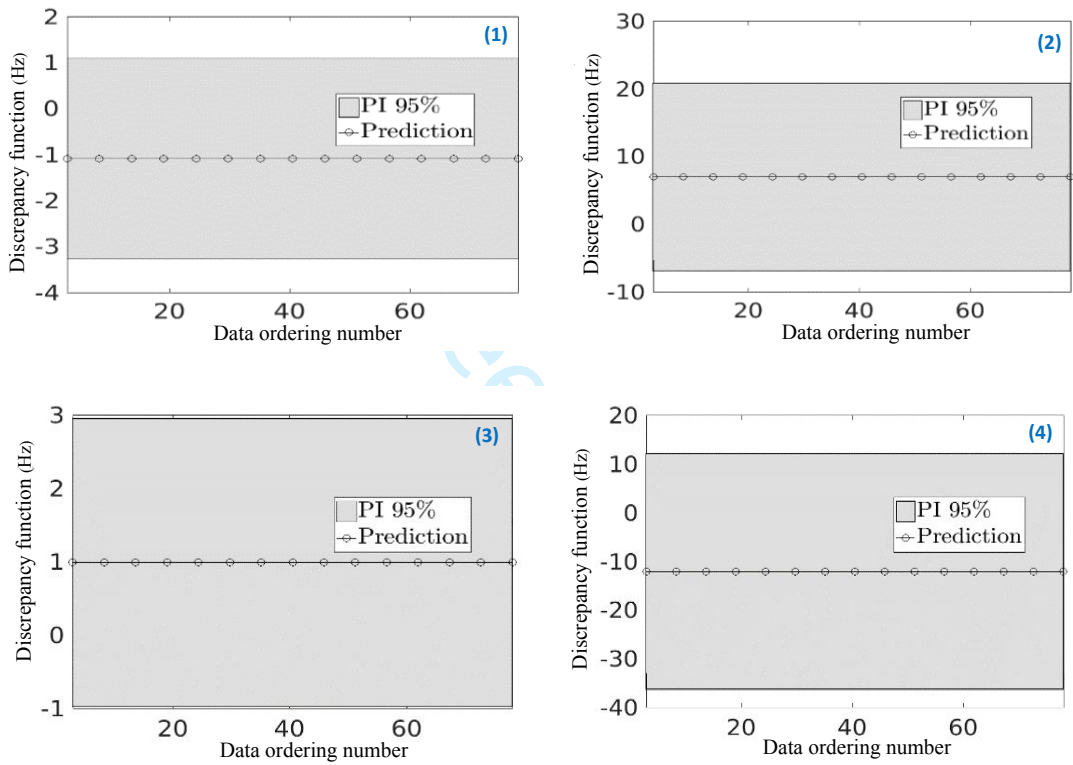
1 As shown in Figure 11, a significant change was targeted at the likelihood in  
2 Young's modulus of the bottom slab, indicating a reduction of about 35.5% to a  
3 new mean value of 20.63 GPa. Further, the decrease in Young's modulus of the  
4 web section was noticeable, showing a likelihood mean of 27 GPa. The impact  
5 forces had little effect on the top slab, and its updated Young's modulus was almost  
6 the same as its initial value. The reduction in the Young's moduli of the bottom  
7 slab and the webs is well matched with the cracks observed in the damaged state,  
8 as mentioned in the section *Two states of box girder bridge*. The discrepancy  
9 functions for all four modes in the damaged state are depicted in Figure 12 (a). As  
10 shown in the figure, the discrepancy increases in the damaged state, especially for  
11 the second and third vertical bending modes. In addition, the discrepancy functions  
12 in the damaged state are distributed more sparsely than those in the undamaged  
13 state. This may be because the cracks cause nonlinearities in the properties of  
14 structural materials and the mechanism of the experimental response.

15 Results of the measured responses together with predicted intervals for all four  
16 modes are shown in Figure 12 (b). As shown, the measured data points are observed  
17 in the corresponding predicted intervals and are very close to the mean values for  
18 all modes except the last one (third vertical bending mode). Results for the third  
19 vertical bending mode are very scattered. It is worth noting that the discrepancy of  
20 this mode is larger than that of the other modes, as shown in Figure 12 (b). This can

1  
2  
3  
4  
5  
6  
7  
8  
9  
10  
11  
12  
13  
14  
15  
16  
17  
18  
19  
20  
21  
22  
23  
24  
25  
26  
27  
28  
29  
30  
31  
32  
33  
34  
35  
36  
37  
38  
39  
40  
41  
42  
43  
44  
45  
46  
47  
48  
49  
50  
51  
52  
53  
54  
55  
56  
57  
58  
59  
60

1 be explained because nonlinearity effects resulting from cracks become more  
2 significant when the vibration mode contains a higher-order curve.

3

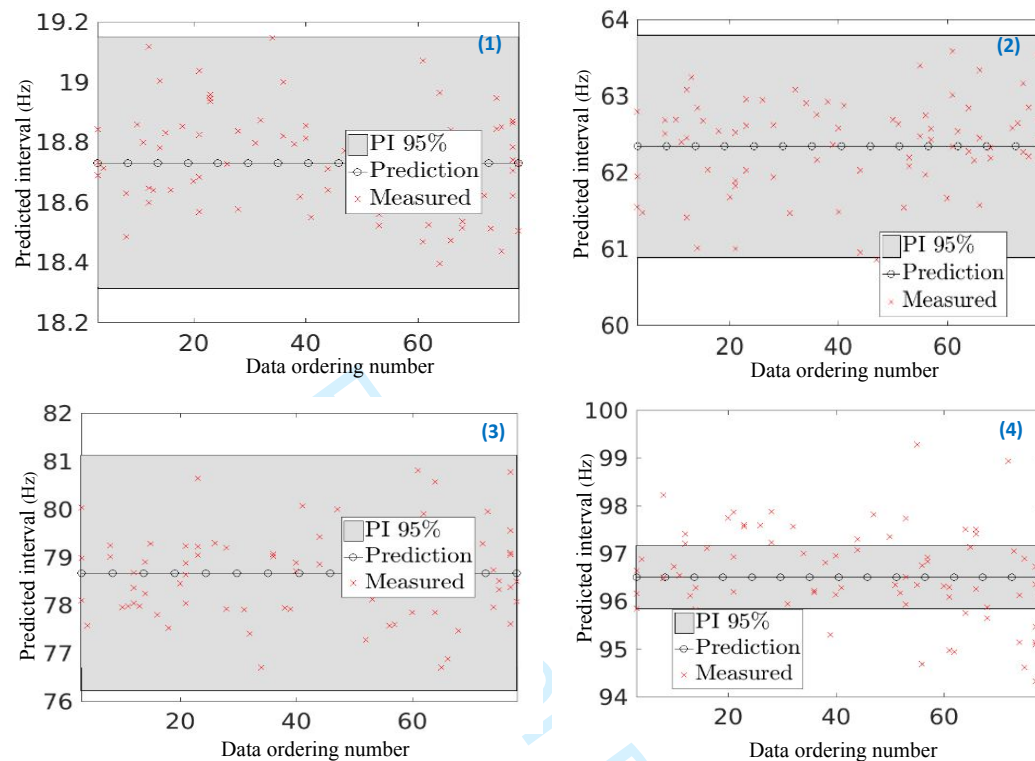


4

5

(a) Discrepancy functions for frequency responses.

6



(b) Predicted interval 95% confidence for numerical model and experimental data points.

**Figure 12.** The results of discrepancy function and predicted response for numerical model in damaged state, for all four modal frequencies as: (1) 1<sup>st</sup> vertical bending frequency, (2) 2<sup>nd</sup> vertical bending frequency, (3) 1<sup>st</sup> lateral bending frequency & (4) 3<sup>rd</sup> vertical bending frequency.

## Conclusions

In this study, the performance of an MBA was investigated in a large lab-scaled BGB using vibration data. Sensitivity analysis was conducted to select the most sensitive parameters and responses. Further, a metamodel was used instead of a

1  
2  
3  
4  
5  
6  
7  
8  
9  
10  
11  
12  
13  
14  
15  
16  
17  
18  
19  
20  
21  
22  
23  
24  
25  
26  
27  
28  
29  
30  
31  
32  
33  
34  
35  
36  
37  
38  
39  
40  
41  
42  
43  
44  
45  
46  
47  
48  
49  
50  
51  
52  
53  
54  
55  
56  
57  
58  
59  
60

1 whole numerical model. Therefore, the computational task and processing time was  
2 reduced in comparison with other probabilistic updating techniques. This benefit  
3 distinguishes this approach, especially in applications to complex structures.

4 This study is the first to apply the MBA for two different states: damaged and  
5 undamaged. These two states represent the health conditions of the structure during  
6 its life span, and the outcomes can be used for further structural investigations.

7 Although a case study is rather simple compared with full-scale real structures, such  
8 a scale provides a possibility to investigate the performance of the proposed  
9 approach in two different states according to the observed evidence on the structure.

10 Further, this study highlighted the advantages of FEMU because it illustrated that  
11 even an FEM of a downscaled structure requires accurate calibration to be reliably  
12 used in further structural assessments.

13 Moreover, in contrast to many previous studies, which applied the MBA to a single  
14 parameter, this study investigated model updating on multiple parameters, such as  
15 material properties and boundary conditions, at the same time. In this study, the  
16 changes to these parameters were well matched with the observed evidence in both  
17 states. Natural frequencies of the first four modes, used as the measured data points,  
18 were predicted correctly. The updated model was sufficiently matched with the  
19 physical observation of the damaged structure. In turn, the results generated from

1 this study might be attributed to the proposed uncertainty quantification  
2 methodology. Further, as the results showed in the damaged state, the discrepancy  
3 functions increased, and experimental responses were not predicted as accurately  
4 as in the undamaged state. Such increases in the discrepancy functions are inferred  
5 as a guide for designers, implying that the FEM needs to be refined by considering  
6 additional aspects such as crack modeling. Further, response prediction can be  
7 improved and discrepancy can be reduced by adding other experimental data points  
8 (e.g., strain and mode shape) and information about environmental conditions (e.g.,  
9 temperature and humidity). Although natural frequency was selected as the  
10 response for the updating process in this study, the MBA is capable of considering  
11 other types of responses. Thus, the performance of the approach when applied to  
12 other responses, such as mode shape, should be investigated in future studies.  
13 Consequently, the proposed methodology contributes to more reliable judgments  
14 about structural safety and more informed maintenance decision-making.

1  
2  
3  
4  
5  
6  
7  
8  
9  
10  
11  
12  
13  
14  
15  
16  
17  
18  
19  
20  
21  
22  
23  
24  
25  
26  
27  
28  
29  
30  
31  
32  
33  
34  
35  
36  
37  
38  
39  
40  
41  
42  
43  
44  
45  
46  
47  
48  
49  
50  
51  
52  
53  
54  
55  
56  
57  
58  
59  
60

## 1 **Acknowledgments**

2 The first author would like to express his sincere appreciation to Queensland  
3 University of Technology (QUT) for the financial support for his research. The support  
4 provided by Australian Research Council (ARC) via a Discovery Project  
5 (DP160101764) is also gratefully acknowledged. Also, the support provided by  
6 technical support from FEMtools is acknowledged.

## 9 **References**

- 10 Arendt, P.D., Apley, D.W. and Chen, W (2012a) Quantification of model uncertainty:  
11 Calibration, model discrepancy, and identifiability. *Journal of Mechanical*  
12 *Design* 134(10):100908-100908-12.
- 13
- 14 Arendt, P.D., Apley, D.W., Chen, W., Lamb, D. and Gorsich, D (2012b) Improving  
15 identifiability in model calibration using multiple responses. *Journal of Mechanical*  
16 *Design* 134(10) 100909-100909-9.
- 17
- 18 Abaqus, F.E.A. (2017) Abaqus Inc. *Providence, Rhode Island, United States.*

- 1  
2  
3  
4  
5  
6  
7  
8  
9 1 Bayarri, M. J., Berger, J. O., Paulo, R., Sacks, J., Cafeo, J. A., Cavendish, J., Lin, C.  
10  
11 2 H., and Tu, J (2007) “A Framework for Validation of Computer Models,”  
12  
13 3 *Technometrics* 49(2), pp. 138–154.  
14  
15  
16 4  
17  
18 5 Beck, J.L. and Au, S.K. (2002) Bayesian updating of structural models and reliability  
19  
20 6 using Markov chain Monte Carlo simulation. *Journal of engineering*  
21  
22 7 *mechanics* 128(4), pp.380-391.  
23  
24  
25 8  
26  
27 9 Beck, J.L. and Katafygiotis, L. S (1998) Updating models and their uncertainties. I:  
28  
29 10 Bayesian statistical framework. *Journal of Engineering Mechanics* 124(4), pp.455-  
30  
31 11 461.  
32  
33  
34 12  
35  
36 13 Conde, B., Eguía, P., Stavroulakis, G.E. and Granada, E. (2018) Parameter  
37  
38 14 identification for damaged condition investigation on masonry arch bridges using a  
39  
40 15 Bayesian approach. *Engineering Structures* 172, pp.275-284.  
41  
42  
43 16  
44  
45 17 Conti, S., Gosling, J.P., Oakley, J.E. and O'Hagan, A. (2009) Gaussian process  
46  
47 18 emulation of dynamic computer codes. *Biometrika* 96(3), pp.663-676.  
48  
49  
50  
51  
52  
53  
54  
55  
56  
57  
58  
59  
60

1  
2  
3  
4  
5  
6  
7  
8  
9  
10  
11  
12  
13  
14  
15  
16  
17  
18  
19  
20  
21  
22  
23  
24  
25  
26  
27  
28  
29  
30  
31  
32  
33  
34  
35  
36  
37  
38  
39  
40  
41  
42  
43  
44  
45  
46  
47  
48  
49  
50  
51  
52  
53  
54  
55  
56  
57  
58  
59  
60

1 Darmawan, M.S. and Stewart, M.G. (2007) Spatial time-dependent reliability analysis  
2 of corroding pretensioned prestressed concrete bridge girders. *Structural Safety* 29(1),  
3 pp.16-31.

4  
5 FEMtools UM (2012) *FEMtools Dynamic Design Solutions* N.V. (DDS)

6  
7 Frangopol, D.M. (2011) Life-cycle performance, management, and optimisation of  
8 structural systems under uncertainty: accomplishments and challenges 1. *Structure*  
9 *and Infrastructure Engineering* 7(6), pp.389-413.

10  
11 Friswell, M. and Mottershead, J.E. (2013) Finite element model updating in structural  
12 dynamics (Vol. 38). Springer Science & Business Media.

13  
14 General principles on reliability for structures (AS 5104)

15  
16 Higdon, D., Gattiker, J., Williams, B. and Rightley, M. (2008) Computer model  
17 calibration using high-dimensional output. *Journal of the American Statistical*  
18 *Association* 103(482), pp.570-583.

19

- 1  
2  
3  
4  
5  
6  
7  
8  
9 1 Jamali, S., Chan, T.H., Nguyen, A. and Thambiratnam, D.P. (2018) Reliability-based  
10  
11 2 load-carrying capacity assessment of bridges using structural health monitoring and  
12  
13 3 nonlinear analysis. *Structural Health Monitoring* 18(1), pp. 20–34.  
14  
15  
16 4  
17  
18 5 Jamali, S., Chan, T.H., Thambiratnam, D.P., Pritchard, R. and Nguyen, A. (2016) Pre-  
19  
20 6 test finite element modelling of box girder overpass-application for bridge condition  
21  
22 7 assessment. In *Australasian Structural Engineering Conference: ASEC 2016* (p. 457).  
23  
24 8 Engineers Australia.  
25  
26  
27 9  
28  
29 10 Jesus, A., Brommer, P., Westgate, R., Koo, K., Brownjohn, J. and Laory, I. (2018)  
30  
31 11 Bayesian structural identification of a long suspension bridge considering temperature  
32  
33 12 and traffic load effects. *Structural Health Monitoring*  
34  
35 13 <https://doi.org/10.1177/1475921718794299>  
36  
37 14  
38  
39 15 Jesus, A., Brommer, P., Westgate, R., Koo, K., Brownjohn, J., & Laory, I. (2019)  
40  
41 16 Modular Bayesian damage detection for complex civil infrastructure. *Journal of Civil*  
42  
43 17 *Structural Health Monitoring* 1-15.  
44  
45  
46  
47  
48  
49  
50  
51  
52  
53  
54  
55  
56  
57  
58  
59  
60

1  
2  
3  
4  
5  
6  
7  
8  
9  
10  
11  
12  
13  
14  
15  
16  
17  
18  
19  
20  
21  
22  
23  
24  
25  
26  
27  
28  
29  
30  
31  
32  
33  
34  
35  
36  
37  
38  
39  
40  
41  
42  
43  
44  
45  
46  
47  
48  
49  
50  
51  
52  
53  
54  
55  
56  
57  
58  
59  
60

- 1 Jesus, A., Brommer, P., Zhu, Y. and Laory, I. (2017) Comprehensive Bayesian  
2 structural identification using temperature variation. *Engineering Structures* 141,  
3 pp.75-82.
- 4
- 5 Jesus, A.H., Dimitrovová, Z. and Silva, M.A. (2014) A statistical analysis of the  
6 dynamic response of a railway viaduct. *Engineering Structures* 71, pp.244-259.
- 7
- 8 Kennedy, M. and O'Hagan, A. (2001a) Bayesian calibration of computer  
9 models. *Journal of the Royal Statistical Society: Series B (Statistical*  
10 *Methodology)* 63(3), pp.425-464.
- 11
- 12 Kennedy, M. and O'Hagan, A. (2001b). Supplementary details on Bayesian calibration  
13 of computer. Rap. tech., University of Nottingham *Statistics Section*.
- 14
- 15 Li, H.N., Li, D.S., Ren, L., Yi, T.H., Jia, Z.G. and Li, K.P. (2016) Structural health  
16 monitoring of innovative civil engineering structures in Mainland China. *Structural*  
17 *Monitoring and Maintenance* 3(1), pp.1-32.
- 18
- 19 Liu, F., Bayarri, M.J. and Berger, J.O. (2009) Modularization in Bayesian analysis,  
20 with emphasis on analysis of computer models. *Bayesian Analysis* 4(1), pp.119-150.

- 1  
2  
3  
4  
5  
6  
7  
8  
9 1 Lophaven, S.N., Nielsen, H.B. and Søndergaard, J. (2002) *DACE: a Matlab kriging*  
10 2 *toolbox* (Vol. 2). IMM, *Informatics and Mathematical Modelling, the Technical*  
11 3 *University of Denmark*.  
12  
13  
14  
15  
16 4  
17  
18 5 Mirza, S.A., Kikuchi, D.K. and MacGregor, J.G. (1980) Flexural strength reduction  
19 6 factor for bonded prestressed concrete beams. In *Journal Proceedings* (Vol. 77, No. 4,  
20 7 pp. 237-246).  
21  
22  
23  
24  
25 8  
26  
27 9 Moravej H, Jamali S, Chan THT, Nguyen A. (2017) Finite element model updating of  
28 10 civil engineering infrastructures: a review literature. *International Conference on*  
29 11 *Structural Health Monitoring of Intelligent Infrastructure. Brisbane, Australia 2017*.  
30  
31  
32  
33  
34 12  
35  
36 13 Mottershead, J.E., Link, M. and Friswell, M.I. (2011) The sensitivity method in finite  
37 14 element model updating: a tutorial. *Mechanical systems and signal processing* 25(7),  
38 15 pp.2275-2296.  
39  
40  
41  
42  
43 16  
44  
45 17 O'Hagan, A. (2006) Bayesian analysis of computer code outputs: A  
46 18 tutorial. *Reliability Engineering & System Safety* 91(10-11), pp.1290-1300.  
47  
48  
49  
50  
51  
52  
53  
54  
55  
56  
57  
58  
59  
60

1  
2  
3  
4  
5  
6  
7  
8  
9  
10  
11  
12  
13  
14  
15  
16  
17  
18  
19  
20  
21  
22  
23  
24  
25  
26  
27  
28  
29  
30  
31  
32  
33  
34  
35  
36  
37  
38  
39  
40  
41  
42  
43  
44  
45  
46  
47  
48  
49  
50  
51  
52  
53  
54  
55  
56  
57  
58  
59  
60

- 1 Pathirage TS. (2017). Identification of prestress force in prestressed concrete box  
2 girder bridges using vibration-based techniques. *Queensland University of*  
3 *Technology*.
- 4
- 5 Rasmussen, C. and Williams, C. (2006) Gaussian Processes for Machine Learning.  
6 *Adaptive Computation and Machine Learning*.
- 7
- 8 Shahidi, S.G. and Pakzad, S.N. (2013) Generalized response surface model updating  
9 using time domain data. *Journal of Structural Engineering* 140(8), p.A4014001.
- 10
- 11 Simoen, E., Papadimitriou, C. and Lombaert, G. (2013) On prediction error correlation  
12 in Bayesian model updating. *Journal of Sound and Vibration* 332(18), pp.4136-4152  
13
- 14 Structural Vibration Solutions A/S (2011) SVS-ARTEMIS Extractor-Release 5.3,  
15 User's manual. Aalborg-Denmark
- 16
- 17 Weng, S., Xia, Y., Zhou, X.Q., Xu, Y.L. and Zhu, H.P. (2012) Inverse substructure  
18 method for model updating of structures. *Journal of Sound and Vibration* 331(25),  
19 pp.5449-5468.

# Vibration-based Bayesian model updating of civil engineering structures applying Gaussian process metamodel

Hossein Moravej, Tommy Chan, Khac-Duy Nguyen and

Andre Jesus

## Abstract

Structural health monitoring plays a significant role in providing information regarding the performance of structures throughout their life spans. However, information that is directly extracted from monitored data is usually susceptible to uncertainties and not reliable enough to be used for structural investigations. Finite element model updating (FEMU) is an accredited framework that reliably identifies structural behavior. Recently, the modular Bayesian approach (MBA) has emerged as a probabilistic technique in calibrating the finite element model (FEM) of structures and comprehensively addressing uncertainties. However, few studies have investigated its performance on real structures. In this paper, MBA is applied to calibrate the FEM of a lab-scaled concrete box girder bridge. This

1  
2  
3  
4  
5  
6  
7  
8  
9  
10  
11  
12  
13  
14  
15  
16  
17  
18  
19  
20  
21  
22  
23  
24  
25  
26  
27  
28  
29  
30  
31  
32  
33  
34  
35  
36  
37  
38  
39  
40  
41  
42  
43  
44  
45  
46  
47  
48  
49  
50  
51  
52  
53  
54  
55  
56  
57  
58  
59  
60

1 study is the first to use the MBA to update the initial FEM of a real structure  
2 for two states—undamaged and damaged conditions—in which the  
3 damaged state represents changes in structural parameters as a result of  
4 aging or overloading. The application of the MBA in the two states provides  
5 an opportunity to examine the performance of the approach with observed  
6 evidence. A discrepancy function is used to identify the deviation between  
7 the outputs of the experimental and numerical models. To alleviate  
8 computational burden, the numerical model and the model discrepancy  
9 function are replaced by Gaussian processes. Results indicate a significant  
10 reduction in the stiffness of concrete in the damaged state, which is identical  
11 to cracks observed on the body of the structure. The discrepancy function  
12 reaches satisfying ranges in both states, which implies that the properties  
13 of the structure are predicted accurately. Consequently, the proposed  
14 methodology contributes to a more reliable judgment about structural  
15 safety.

16

## 17 **Keywords**

18 Finite Element Model Updating, Bayesian framework, Gaussian process,  
19 Structural Health Monitoring, Box girder bridge, Vibration analysis

20

## 1 Introduction

2 Civil infrastructure plays a significant role in keeping urban systems operational, but  
3 any malfunctions in routine performance can result in major hazards and even threaten  
4 lives. Therefore, it is important to regularly investigate the safety of infrastructure.  
5 Many researchers such as Frangopol (2011) and Li et al. (2016) have acknowledged  
6 the importance of monitoring the behaviors of structures using information provided  
7 by structural health monitoring (SHM). An accredited approach to addressing the  
8 aforementioned objective is finite element model updating (FEMU), which aims to  
9 improve the accuracy of the finite element models (FEMs) of real structures and  
10 reduce the discrepancy between the output of FEMs and experimental measurements.  
11 The availability of reliable FEMs of structures is beneficial in terms of evaluation of  
12 structural performance, reliability analysis, load-carrying capacity assessment, and  
13 damage detection.  
14 However, FEMU faces significant barriers that prevent it from reaching its peak  
15 efficiency. For example, computational burden, especially in the case of complex  
16 structures, makes this technique cumbersome, and in some cases, the process of  
17 updating may lead to ill-conditioned optimization problems with limited practical  
18 applicability. Although some approaches have recently been introduced to improve  
19 computational efficiency, such as the response surface method (Shahidi and Pakzad,

1  
2  
3  
4  
5  
6  
7  
8  
9  
10  
11  
12  
13  
14  
15  
16  
17  
18  
19  
20  
21  
22  
23  
24  
25  
26  
27  
28  
29  
30  
31  
32  
33  
34  
35  
36  
37  
38  
39  
40  
41  
42  
43  
44  
45  
46  
47  
48  
49  
50  
51  
52  
53  
54  
55  
56  
57  
58  
59  
60

1 2013) and the substructure technique (Weng et al., 2012), this challenge still needs to  
2 be addressed.

3 Another challenge when updating a model relates to addressing different sources  
4 of uncertainties. To overcome this problem, probabilistic approaches that are more  
5 reliable than their deterministic counterparts have been introduced in the field of  
6 FEMU (Jesus et al., 2014; Jesus et al., 2018). Deterministic techniques, which  
7 consider fixed values regarding input parameters and response outputs, rarely  
8 provide a satisfactory correlation between the numerical model and real data  
9 because of inherent structural uncertainties (Friswell and Mottershead, 2013). In  
10 contrast, probabilistic approaches do not regard input parameters as fixed numbers  
11 to lock the updating process in those values; instead, they consider a realistic  
12 statistical distribution for each parameter. This consideration is more logical  
13 because it is impossible to confidently assert a certain value for one parameter using  
14 an updating process because of the existence of uncertainties. Therefore, in most  
15 cases, probabilistic approaches are more reliable. According to Kennedy and  
16 O'Hagan (2001a, 2001b), the main sources of uncertainty in model prediction are  
17 uncertainty in model parameters, modeling errors, and uncertainty resulting from  
18 observation errors. Uncertainty in model parameters relates to inputs to the  
19 computer model that are unknown and cannot be identified directly from physical  
20 experiments, such as the material properties of a damaged structure. Another source

1  
2  
3  
4  
5  
6  
7  
8  
9 1 of uncertainty—modeling error or model inadequacy—refers to any assumptions  
10  
11 2 or simplifications made while developing FEMs, such as considering a material  
12  
13 3 linear, isotropic, and homogenous. This source of uncertainty occurs even when all  
14  
15 4 parameters are accurately identified. The observation error (i.e., experimental  
16  
17 5 uncertainty) is usually present in physical experiments. This type of uncertainty  
18  
19 6 denotes variations that may occur in the experimental measurement even when the  
20  
21 7 test is repeated with the same settings.  
22  
23  
24

25 8 Despite the significant effects of the abovementioned uncertainties, few studies  
26  
27 9 have addressed all of these aspects. A number of probabilistic approaches have  
28  
29 10 been developed in FEMU, including the fuzzy number-based method, Kalman  
30  
31 11 Filter-based technique, model falsification diagnosis method, Markov process-  
32  
33 12 based method and sampling method. Among all probabilistic FEMU techniques,  
34  
35 13 Bayesian updating has been found to be one of the most applicable approaches for  
36  
37 14 updating FEMs. Several attempts have been made to apply Bayesian updating, and  
38  
39 15 Beck's method is eminent among them because it proposes a robust predictive  
40  
41 16 approach (Beck and Katafygiotis, 1998; Beck and Au, 2002). The major weakness  
42  
43 17 in the presentation of Bayesian methods in SHM practices is that uncertainty  
44  
45 18 resulting from modeling errors is not properly considered. Only a few researchers  
46  
47 19 have performed the Bayesian approach with consideration of this aspect (Higdon  
48  
49 20 et al., 2008; Simoen et al., 2013). Higdon used a comprehensive modular Bayesian  
50  
51  
52  
53  
54  
55  
56  
57  
58  
59  
60

1 approach (MBA) that was formerly established by Kennedy and O'Hagan (2001a),  
2 but it was not generally successful in addressing identifiability. Identifiability  
3 represents the ability to achieve the true value of model parameters based on  
4 available data to illustrate a physical property such as Young's modulus (Arendt et  
5 al., 2012a). Arendt et al. (2012b) proposed an improvement to Kennedy and  
6 O'Hagan's original formulation using the MBA to overcome the identifiability  
7 problem by applying measured data with various responses. This method replaces  
8 an FEM with a Gaussian process (GP) model as a metamodel (Kennedy and  
9 O'Hagan, 2001a). It has been found that the method significantly reduces  
10 computational effort—especially in cases of complex structures (Lophaven et al.,  
11 2002; Jesus et al., 2017; Conde et al., 2019; Jesus et al., 2019). The GP model  
12 for interpolation that considers uncertainties is found to be effective, even if data  
13 are limited. This formulation is preferable to former studies in model updating  
14 because it comprises the main sources of uncertainties and consequently reaches  
15 more realistic outcomes.

16 Based on the thriving interest in the MBA, this study validates its practical  
17 performance in FEMU by means of measured vibration data. The study investigates  
18 the applicability of the algorithm to a lab-scaled reinforced concrete box girder  
19 bridge (BGB), which represents a typical hollow core bridge deck in Australia. The  
20 MBA is applied in two states—undamaged and damaged—to calibrate multiple

1 parameters of the FEM. The performance of the approach is examined according  
2 to the observed evidence of the undamaged condition with initial minor cracks and  
3 the damaged condition with imposed cracks. The damaged state represents changes  
4 in structural parameters as a result of aging or overloading. Accordingly, this study  
5 aims to identify changes in the structural parameters and provide a reliable updated  
6 model for each state. The structural identification provided through the applied  
7 framework will not only provide a better understanding of structural performance,  
8 but will also contribute to providing suitable guidelines for decision-making  
9 regarding maintenance actions.

10

## 11 **Model Updating Methodology**

12 This section describes the model updating approach used in this study. The first  
13 subsection explains the connecting equation between the observations and the outputs  
14 of the numerical model. The second subsection briefly presents the GP, and the last  
15 subsection outlines the framework.

16

17

18

1  
2  
3  
4  
5  
6  
7  
8  
9 **1** *Observation and numerical model relationship*

10  
11  
12 **2** We assume that a real and unobservable process  $f$  has  $n$  observations of  $q$  responses

13  
14 **3**  $\mathbf{Y}^e$  from the measured data, where the superscript “ $e$ ” is the experimental model.

15  
16  
17 **4** The relationship between  $f$  and  $\mathbf{Y}^e$  can be denoted as equation (1):

18  
19  
20  
21  
22  
23 **6** 
$$\mathbf{Y}^e = \mathbf{f} + \boldsymbol{\varepsilon} \tag{1}$$

24  
25  
26  
27  
28 **8** where  $\boldsymbol{\varepsilon} = [\varepsilon_1, \dots, \varepsilon_n]^T$  is the observation error, which is supposed to work as a

29  
30 **9** Gaussian distribution with a mean of 0 and variance of  $\Lambda \in \mathbb{R}$ . Alternatively, the

31  
32  
33 **10** real process  $f$  can be interpreted as equation (2) to comprise the numerical model:

34  
35  
36  
37  
38  
39 **12** 
$$\mathbf{f} = \mathbf{Y}^m(\boldsymbol{\theta}^*) + \boldsymbol{\delta} \tag{2}$$

40  
41  
42  
43  
44 **14** where  $\boldsymbol{\delta}$  is a discrepancy function that represents the difference between the

45  
46 **15** numerical model and the real process.  $\mathbf{Y}^m(\boldsymbol{\theta}^*)$  is the numerical model’s output and

47  
48 **16**  $\boldsymbol{\theta}^*$  is an  $r$ -dimensional vector of the true structural parameters. This equation is an

49  
50 **17** idealized form of the final model (i.e., the model after successful calibration), while

51  
52  
53 **18** the model parameters  $\boldsymbol{\theta}$  take the values  $\boldsymbol{\theta}^*$ . Significantly, the discrepancy function

1  
2  
3  
4  
5  
6  
7  
8  
9 does not depend on the model's output and is an unknown in addition to the  
10 structural parameters. Equation (2) is then substituted into equation (1) to obtain  
11  
12  
13  
14 equation (3):

$$15 \quad \mathbf{Y}^e = \mathbf{Y}^m(\theta^*) + \boldsymbol{\delta} + \boldsymbol{\varepsilon} \quad (3)$$

16  
17  
18  
19  
20  
21  
22  
23  
24 Equation (3) is a comprehensive equation of the model updating process. It denotes  
25  
26  
27  
28  
29  
30  
31  
32  
33  
34  
35  
36  
37  
38  
39  
40  
41  
42  
43  
44  
45  
46  
47  
48  
49  
50  
51  
52  
53  
54  
55  
56  
57  
58  
59  
60  
the output of the processes within the domain of a calibrated status  $\theta = \theta^*$ , which  
implies the best fit compared with the observed data.

10 In the next step, the numerical model and the discrepancy function are substituted  
11  
12  
13  
14  
15  
16  
17  
18  
19  
20  
21  
22  
23  
24  
25  
26  
27  
28  
29  
30  
31  
32  
33  
34  
35  
36  
37  
38  
39  
40  
41  
42  
43  
44  
45  
46  
47  
48  
49  
50  
51  
52  
53  
54  
55  
56  
57  
58  
59  
60  
with two multiple-response Gaussian processes (MRGPs) whose hyperparameters  
must be found. These hyperparameters describe the MRGPs and illustrate the  
approximation of their associated uncertainties such as variability of the numerical  
model, modeling discrepancies, and observation errors.

### 16 *Gaussian Process*

17 Gaussian processes (GP) modeling is an interpolation approach that considers  
18  
19  
20  
21  
22  
23  
24  
25  
26  
27  
28  
29  
30  
31  
32  
33  
34  
35  
36  
37  
38  
39  
40  
41  
42  
43  
44  
45  
46  
47  
48  
49  
50  
51  
52  
53  
54  
55  
56  
57  
58  
59  
60  
uncertainty highly efficient even when data are limited (Kennedy and O'Hagan,  
2001a; Rasmussen et al., 2006). By applying interpolations and extrapolations, this

1  
2  
3  
4  
5  
6  
7  
8  
9  
10  
11  
12  
13  
14  
15  
16  
17  
18  
19  
20  
21  
22  
23  
24  
25  
26  
27  
28  
29  
30  
31  
32  
33  
34  
35  
36  
37  
38  
39  
40  
41  
42  
43  
44  
45  
46  
47  
48  
49  
50  
51  
52  
53  
54  
55  
56  
57  
58  
59  
60

1 approach offers a predicted GP that is fitted on all observation points. In this study,  
2 an MRGP is applied by assuming that the metamodel of model  $\mathbf{Y}$  is a single  
3 realization of a spatial random process with a prior mean function and covariance  
4 function (O'Hagan, 2006; Rasmussen et al., 2006). Regarding approximation of the  
5 metamodel, it is assumed that a dataset of  $\mathbf{Y}$  with a size of  $g$  and  $N$  observations  
6 should be available as input. Dimension  $g$  represents the number of responses ( $Y_1,$   
7  $Y_2, \dots, Y_g$ ). To generate the MRGP, the mean function is required to be obtained,  
8 which exists at every design input point without uncertainty. In the spaces located  
9 between or outside the design input points, the MRGP will produce either a possible  
10 interpolation or extrapolation from the existing data points.

11 In the MRGP, the prior mean function is supposed to be a member of a hierarchical  
12 structure of linear functions. It can be generalized as the form  $\mathbf{M}=\mathbf{H}\boldsymbol{\beta}$ . Herein,  
13 matrix  $\mathbf{H}$  comprises  $N$  polynomial constant regression functions and the matrix of  
14 regression coefficient  $\boldsymbol{\beta}$  for each term included in matrix  $\mathbf{H}$  and each fitted response  
15 in  $\mathbf{Y}$ . That is,  $\mathbf{H}$  is a row vector of regression functions and  $\boldsymbol{\beta}$  is a column vector of  
16 regression functions.

17 The prior covariance function of the MRGP for the model and discrepancy function  
18 can be formulated as equation (4):

19

$$\mathbf{V} = \Sigma^2 \otimes \mathbf{R} \quad (4)$$

where  $\mathbf{V}$  is covariance function,  $\Sigma^2 \in \mathbb{R}^{g \times g}$  is a non-temporal variance matrix, and  $\mathbf{R} \in \mathbb{R}^{N \times N}$  is a temporal correlation matrix, and  $\otimes$  is the Kronecker product operation on the two matrices. This equation can be interpreted as the separation of a variance between the  $g$  responses (which are being approximated) and a correlation between the  $N$  times histories. Each entry of Matrix  $\mathbf{R}$  contains a correlation function that needs to be approximated. This assumption is applicable to the correlation function of the numerical model. In addition, because the FEM is linear, a linear correlation function is assumed for the correlation function in this study, as shown in equation (5). This model fits properly to the data and is numerically stable (Lophaven et al., 2002).

$$\mathbf{R}(\omega, \theta, \theta') = \prod_{j=1}^r \max\{0, 1 - \omega_j |\theta_j - \theta'_j|\} \quad (5)$$

In equation (5),  $\omega_j$  ( $j=1, \dots, r$ ) is the roughness parameter and represents how roughly the responses change from point  $\theta$  to point  $\theta'$  for each of the structural parameters of interest.

In contrast, the correlation matrix for the discrepancy function is simply assumed as an identity matrix as  $\mathbf{R}=\mathbf{I}$ . This assumption implies that the final predicted

1 responses have no temporal correlation. This is reasonable for natural frequencies  
 2 obtained from a laboratory model because they vary randomly without any definite  
 3 relations. The final hyperparameter that needs to be estimated to conclude the  
 4 description of the MRGP is  $\Lambda$  as the  $N \times 1$  variance vector of the observation error  
 5  $\varepsilon$ , which can simply be added to equation (4) to reach equation (6).

$$6 \quad \mathbf{V} = \Sigma^2 \otimes \mathbf{R} + \Lambda \quad (6)$$

7  
 8  
 9  
 10 After providing a certain amount of data  $\mathbf{Y}$ , the MRGP is provided (supposing a non-  
 11 informative prior for  $\beta$  and given  $\omega$  and  $\Sigma$ ). The posterior distribution of the response  
 12 is given by equation (7):

$$13 \quad y | \Sigma, \omega, \Lambda, \mathbf{Y} \sim N(m^*, \Sigma \otimes \mathbf{y}^*) \quad (7)$$

14 with

$$15 \quad m^* = h\hat{\beta} + \mathbf{y}^T \Gamma^{-1} (\mathbf{Y} - \mathbf{H} \hat{\beta}) \quad (8)$$

$$16 \quad \mathbf{y}^* = \mathbf{y} - \mathbf{y}^T \Gamma^{-1} \mathbf{y} + [h^T - \mathbf{H}^T \Gamma^{-1} \mathbf{y}]^T [\mathbf{H}^T \Gamma^{-1} \mathbf{H}]^{-1} [h^T - \mathbf{H}^T \Gamma^{-1} \mathbf{y}] \quad (9)$$

1 where  $y$  represents the MRGP,  $h$  is the hierarchical structure of regression  
 2 functions.  $\gamma$  is defined as a relational correlation matrix, which maps the correlation  
 3 between the indices of points of available dataset and the indices of points supposed  
 4 to be predicted (Conti et al., 2009). The used correlation function is the same as  
 5 equation (5).  $\hat{\beta}$  stands for the estimated matrix of  $\beta$  and is given by calculating  
 6 equation (10):

$$\mathbf{H}^T \mathbf{R}^{-1} \mathbf{H} \hat{\beta} = \mathbf{H}^T \mathbf{R}^{-1} \mathbf{Y} \quad (10)$$

7  
 8  
 9 which refers to the linear regression solution of the best linear unbiased predictor.  
 10  $\Gamma$  is an  $N \times N$  correlation matrix that contains the linear functions. The MRGP in  
 11 equation (7) can be defined by estimating the hyperparameters  $\omega$ ,  $\beta$ ,  $\Sigma$ , and  $\Lambda$ .  
 12 Characterization of the hyperparameters can be conducted using a Bayesian  
 13 approach, which would address all of the mentioned uncertainties and identify all  
 14 of the hyperparameters at the same time. However, this approach is not efficient  
 15 because it comprises a huge computational process (Liu et al., 2009). Therefore,  
 16 for better computational efficiency, the hyperparameters are calculated with the  
 17 maximum likelihood estimations (MLEs). A more comprehensive description of  
 18 the GP method can be found in Arendt et al. (2012a).  
 19

1  
2  
3  
4  
5  
6  
7  
8  
9  
10  
11  
12  
13  
14  
15  
16  
17  
18  
19  
20  
21  
22  
23  
24  
25  
26  
27  
28  
29  
30  
31  
32  
33  
34  
35  
36  
37  
38  
39  
40  
41  
42  
43  
44  
45  
46  
47  
48  
49  
50  
51  
52  
53  
54  
55  
56  
57  
58  
59  
60

## 1 *Modular Bayesian approach (MBA)*

2 The MBA separates the updating process into four steps. The hyperparameters of  
3 the MRGP are approximated separately and consecutively, as shown in Figure 5 in  
4 the study by Arendt et al. (2012a). In the MBA, the hyperparameters continue to be  
5 estimated until the first order of uncertainties is found, and then they are fixed. It is  
6 worth noting that setting up the hyperparameters at fixed estimations decreases the  
7 degree of approximation of the uncertainties. In addition, the “second-order”  
8 resolution of the uncertainties is ignored to alleviate the computational burden and  
9 make it faster than fully considering the uncertainties in the Bayesian framework.  
10 This act of estimating and fixing the hyperparameters is performed sequentially  
11 when progressing from module 1 to module 2 and from module 2 to module 3.

12 The first module basically substitutes the computer model to an MRGP model and  
13 estimates its hyperparameters based on only the simulation data. In this module,  
14 the simulation is run in finite element modeling software (e.g., Abaqus) to obtain  
15 the simulated responses by randomly changing the input parameters using Latin  
16 hypercube sampling (LHS). For the experimental validation in this study, 120 and  
17 80 runs were conducted in the undamaged and damaged states, respectively, to  
18 provide a dataset. The estimation can be carried out using numerical optimization  
19 methods by fitting a likelihood between the MRGP and the available simulation

1  
2  
3  
4  
5  
6  
7  
8  
9  
10  
11  
12  
13  
14  
15  
16  
17  
18  
19  
20  
21  
22  
23  
24  
25  
26  
27  
28  
29  
30  
31  
32  
33  
34  
35  
36  
37  
38  
39  
40  
41  
42  
43  
44  
45  
46  
47  
48  
49  
50  
51  
52  
53  
54  
55  
56  
57  
58  
59  
60

1 data. In this study, a genetic algorithm (GA) routine was applied in MATLAB. For  
2 the GA setup, an initial population of size 40 is generated in the [0; 1] range, a  
3 Gaussian mutation function with a scale of 1 (i.e., initial standard deviation of 1)  
4 and a standard deviation shrink of 1 is chosen, and a scattered crossover function  
5 applied to a portion of 0.8 of the population at each generation is defined.  
6 Convergence criteria are set as either a maximum number of 100 generations or  
7 until an average change in the fitness value of  $1 \times 10^{-6}$  is reached.

8 In module 2, the discrepancy function is estimated by fitting another MRGP model  
9 according to the measured data from the experiment, the simulation data, and the  
10 prior distribution of the calibration parameters. The GA is used to approximate the  
11 discrepancy function by estimating the hyperparameters of the GP. This task is  
12 carried out by an MLE, which indicates that the fitness function of the GA is a  
13 likelihood function. It should be mentioned that either the MBA or the full Bayesian  
14 approach can estimate the hyperparameters of the abovementioned MRGP models  
15 through MLE and Bayesian posterior distributions, respectively. As discussed in  
16 the previous section, the MBA is used in this study because Bayesian posterior  
17 distributions can be computationally inefficient. In addition, according to Bayarri  
18 et al. (2007), both approaches have similar results in predicting the discrepancy  
19 function and calibration parameters.

1  
2  
3  
4  
5  
6  
7  
8  
9  
10  
11  
12  
13  
14  
15  
16  
17  
18  
19  
20  
21  
22  
23  
24  
25  
26  
27  
28  
29  
30  
31  
32  
33  
34  
35  
36  
37  
38  
39  
40  
41  
42  
43  
44  
45  
46  
47  
48  
49  
50  
51  
52  
53  
54  
55  
56  
57  
58  
59  
60

1 In module 3, Bayes' theorem is applied to approximate the posterior distribution of  
2 the updated parameters and its likelihood function containing the two MRGP  
3 models approximated in modules 1 and 2. Since multiple parameters are calibrated  
4 in this study, a Markov chain Monte Carlo method can be used to estimate the  
5 MBA. This choice implies that a target distribution must be used, and in this study,  
6 a multivariate normal distribution is chosen (Arendt et al., 2012b).

7 In module 4, the experimental responses are calculated by applying the measured  
8 data and the estimated hyperparameters obtained from modules 1 and 2. After the  
9 simulated and measured data are collected in modules 1 and 2 and the calibrated  
10 parameters are estimated in module 3, the posterior distribution response of the  
11 updated model together with the updated discrepancy function can be obtained. For  
12 the prediction of the responses, 40 measured data points for the undamaged state  
13 and 60 data points for the damaged state are randomly distributed along the  
14 simulated data points. It is worth noting that simulated data have been provided by  
15 applying the LHS approach as described in the first module. In addition, it is  
16 assumed that the measured responses are independent of time, temperature  
17 variation, and other operational effects.

18  
19  
20

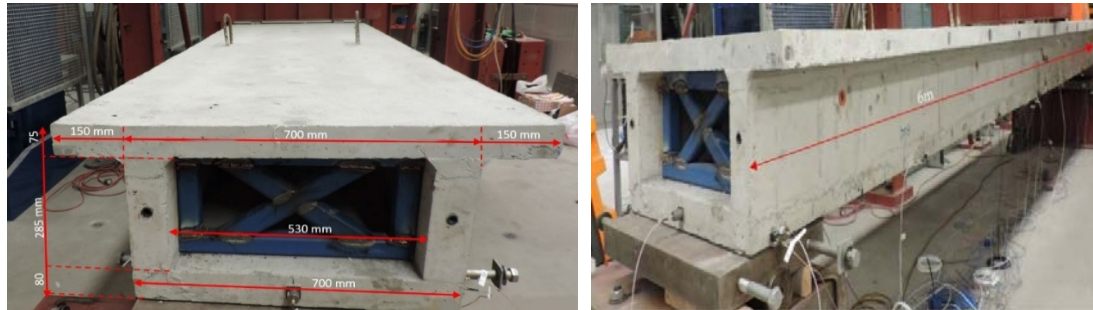
## 1 **Finite element model updating for a box girder bridge**

2 The first subsection presents details of the BGB and two different states (i.e.,  
3 undamaged and damaged) of the structure. Details of an FEM and experimental  
4 modal analysis as two counterparts in model updating are provided in the second  
5 and third subsections, respectively. The fourth subsection highlights sensitivity  
6 analysis as a tool to select appropriate parameters and responses in FEMU.

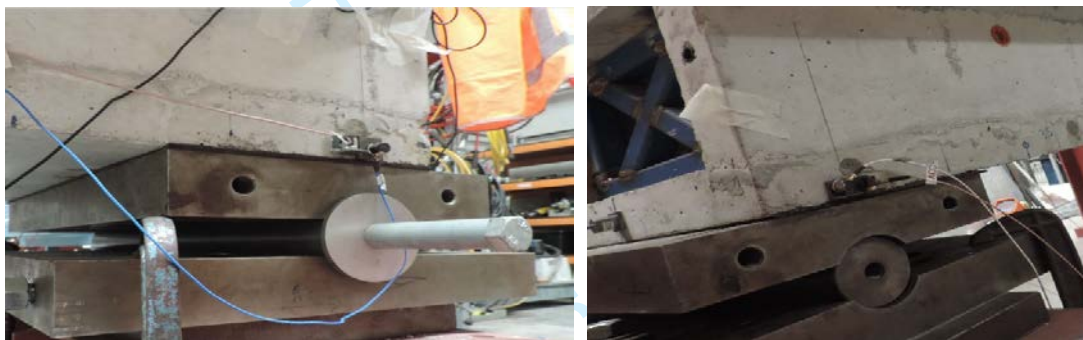
### 7 8 *Two states of box girder bridge*

9 A downscaled reinforced concrete BGB, which was constructed in the civil  
10 engineering laboratory at the Queensland University of Technology, is investigated  
11 in this study. This structure represents a typical in-service hollow core bridge deck  
12 in Australia. The length of the BGB is 6 m, and it was cast in three separate parts  
13 as the bottom slab, the webs, and the top slab. Detailed dimensions of the structure  
14 are shown in Figure 1 (a). Further information about the casting steps can be found  
15 in Pathirage (2017). The BGB was placed on two simple supports as a pin at one  
16 end and a roller at the other end, as shown in Figure 1 (b). This platform refers to  
17 the undamaged state (first state), despite the existence of some minor cracks  
18 beneath the soffit slab.

19



(a)



(b)

**Figure 1.** The BGB details: (a) BGB's dimensions and (b) Boundary conditions in BGB as Roller (left) and Pin (right).

In the second state (damaged state), a point load and then a cyclic load were applied at the midspan of the BGB. These impacts resulted in some significant cracks on the soffit slab and the webs of the BGB. Eight significant cracks were observed, each of which ran through the whole width of the bottom slab and propagated to the webs. Figure 2 shows some observed cracks on the body of the structure.

1

2

3

4

5

6

7

8

9

10

11

12

13

14

15

16

17

18

19

20

21

22

23

24

25

26

27

28

29

30

31

32

33

34

35

36

37

38

39

40

41

42

43

44

45

46

47

48

49

50

51

52

53

54

55

56

57

58

59

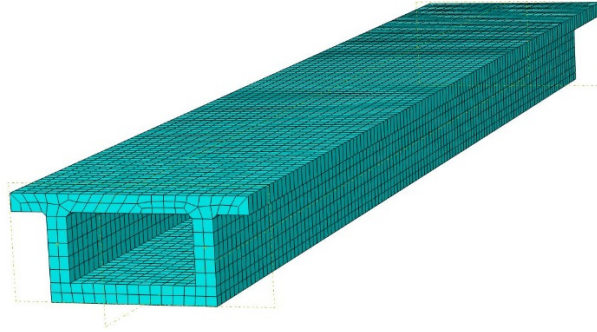
60



**Figure 2.** Detected cracks on body of the BGB in damaged state.

### *Numerical model*

Given the lack of available information about the structural parameters of the BGB, such as material properties and boundary conditions, nominal values of the parameters were assumed from the designing details and were used to create a numerical model of the BGB. The initial BGB's FEM was built in the Abaqus software package, as shown in Figure 3 (Abaqus, 2017).



1  
2  
3  
4  
5  
6  
7  
8  
9  
10  
11  
12  
13  
14  
15  
16  
17  
18  
19  
20  
21  
22  
23  
24  
25  
26  
27  
28  
29  
30  
31  
32  
33  
34  
35  
36  
37  
38  
39  
40  
41  
42  
43  
44  
45  
46  
47  
48  
49  
50  
51  
52  
53  
54  
55  
56  
57  
58  
59  
60

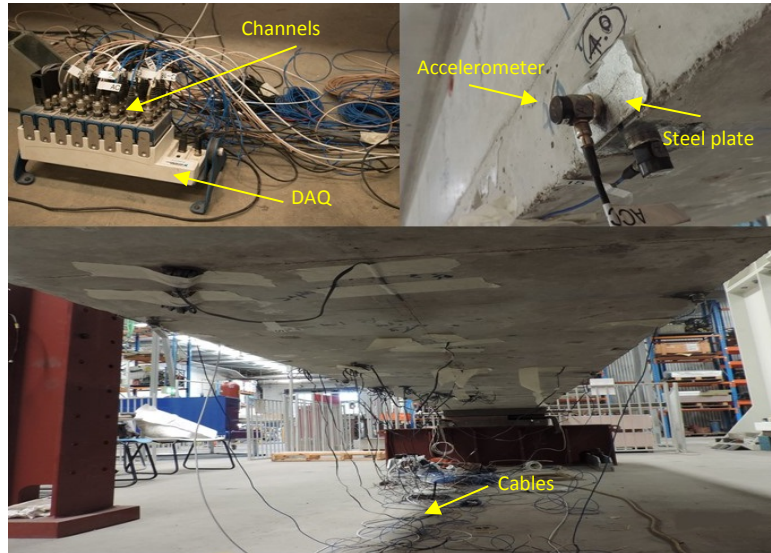
**Figure 3.** FEM of BGB built in ABAQUS 2017.

From the Abaqus element library, a C3D8R solid element and a T3D2 truss element were assigned to the concrete and reinforcement elements, respectively. Regarding material properties, according to the design details, Young's modulus ( $E$ ) is assumed as 200 (GPa) for reinforcement and 32 (GPa) for concrete. Further, mass density ( $\rho$ ) is assumed as  $7,850 \text{ kg/m}^3$  for reinforcement and  $2,400 \text{ kg/m}^3$  for concrete. In addition, the boundary conditions were considered fixed in vertical displacement for both supports. In this study, a convergence assessment for mesh size selection was performed by applying a load-displacement control. Herein, load against midspan deflection was examined for different mesh sizes. A mesh size of 50 mm was determined to be fit enough by considering the experimental displacement at the mid-zone in failure mode. More details of the analysis can be found in Jamali et al. (2018). In this study, four natural frequencies of the FEM—first vertical bending, second vertical bending, first lateral bending, and third vertical bending modes—were selected

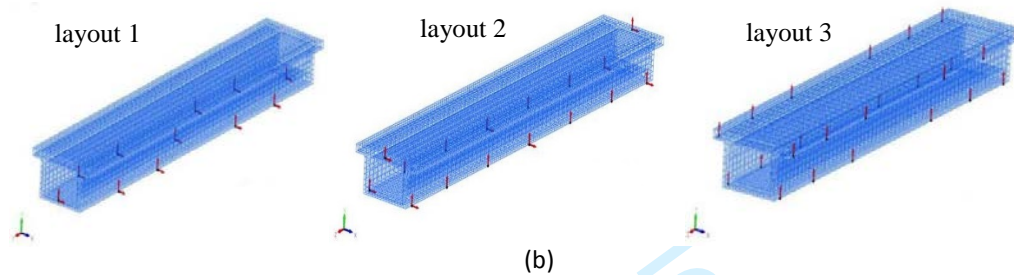
1  
2  
3  
4  
5  
6  
7  
8  
9 1 and used to update the FEM because similar mode shapes and natural frequencies were  
10  
11 2 extracted from the measured data.  
12  
13  
14 3

#### 16 4 *Modal data analysis*

18 5 During the casting process of the BGB, several small steel plates were attached to  
19 6 the BGB's surface to facilitate sensor installation. The sensory system used in this  
20 7 study is shown in Figure 4 (a). Regarding the selection of the right sensor layout,  
21 8 different aspects were noticed in relation to the number and type of available  
22 9 sensors, the excitation source, and the maximum number of channels in the data  
23 10 acquisition system. More details regarding the preparation of the experiment can  
24 11 be found in Jamali et al. (2016). The BGB was excited by applying multipoint  
25 12 random excitation with an impact hammer for each vibration test. Vibration  
26 13 responses were recorded using a data acquisition system. In this study, the vibration  
27 14 responses of the structure in both the undamaged and damaged states were  
28 15 measured and used in the FEMU process. Figure 4 (b) shows three examples of  
29 16 sensor layout arrangements that were applied in the modal analysis in this research.  
30 17 Each arrow in the figure represents a single sensor in the corresponding direction.  
31  
32  
33  
34  
35  
36  
37  
38  
39  
40  
41  
42  
43  
44  
45  
46  
47  
48  
49  
50  
51  
52  
53  
54  
55  
56  
57  
58  
59  
60



(a)

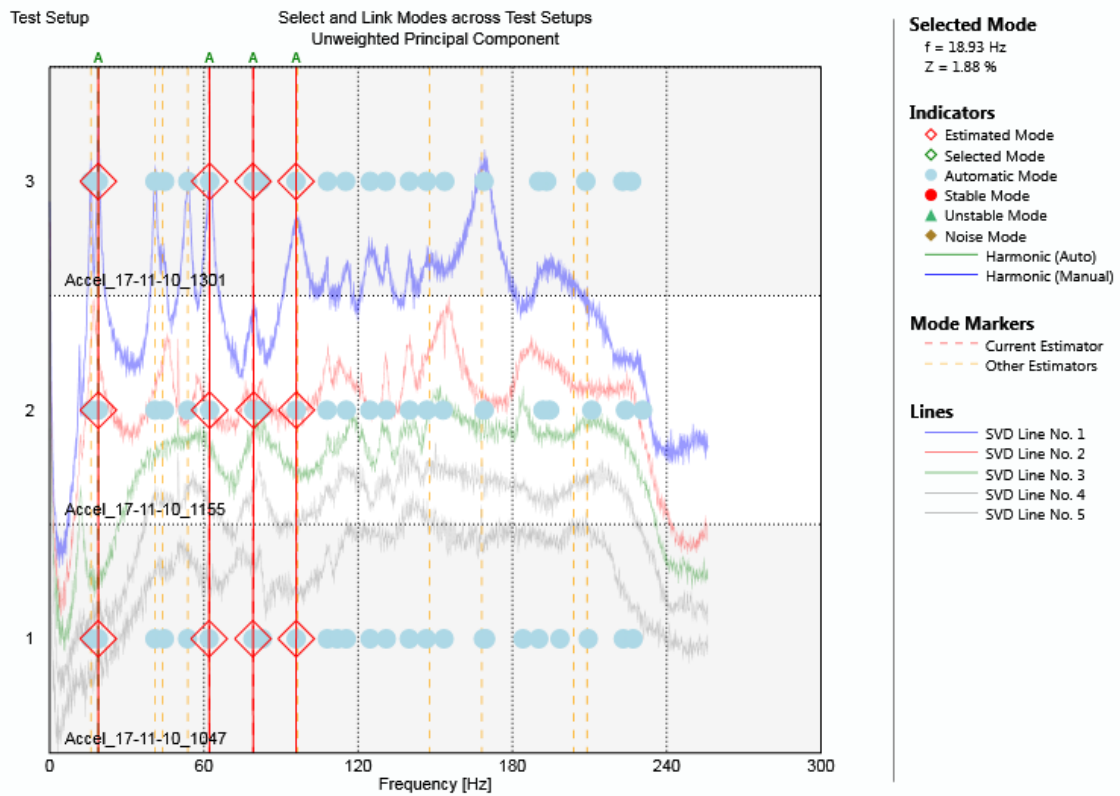


(b)

**Figure 4.** Structural response measurement: (a) Sensory system on the BGB and (b) Sensor layouts.

The measured acceleration responses were post-processed in the modal analysis step. In this regard, the stochastic subspace identification (SSI) method, which is embedded in the ARTeMIS Modal software package, was applied (ARTeMIS, 2011). An example of modal analysis for a dataset is illustrated in Figure 5.

1



2

3

Figure 5. Modal Analysis to capture experimental frequency in ARTeMIS.

4

5 Modal parameters for 40 datasets in the undamaged state and 60 datasets in the  
 6 damaged state were analyzed. The test was conducted in a controlled environment  
 7 in the laboratory, where ambient effects had little effect on the measured responses;  
 8 therefore, the number of modal analyses in both states was sufficient. The detected  
 9 natural frequencies were the first vertical bending, second vertical bending, first

5

6

7

8

9

10

11

12

13

14

15

16

1 lateral bending, and third vertical bending modes, similar to the FEM's results.  
 2 These modes were selected for the FEMU process because they could be detected  
 3 in both the undamaged and damaged states. The four measured mode shapes were  
 4 transferred into the FEMtools software package (Dynamic Design Solutions,  
 5 2012). The number of degrees of freedom (DOF) of an experimental model is often  
 6 smaller than that of the corresponding FEM as a result of a lack of available sensors  
 7 (Moravej et al., 2017). In this study, a coordinate expansion technique was applied  
 8 to increase the number of DOFs of the experimental model to the same number in  
 9 the FEM (Moravej et al., 2017). The values of the natural frequencies in both states  
 10 are shown in Table 1. In this table, the mode order refers to the ordering number of  
 11 the modes. The experimental and numerical mode shapes are illustrated in Figure  
 12 6.

13  
 14 **Table 1.** Frequency in the initial designed model and measured frequency in two states

Mode order	Freq as Designed (Hz)	Measured Freq (Undamaged)		Error (%)	Measured Freq (Damaged)		Error (%)
		Mean value (Hz)	STD		Mean value (Hz)	STD	
1	24.339	21.65	0.106	-12.42	18.78	0.082	-29.60
2	81.29	67.06	0.21	-21.22	63.06	0.174	-28.9
3	92.108	84.32	0.124	-9.24	80.73	0.14	-14.09
4	109.75	98.21	0.18	-11.75	95.74	1.023	-14.63

15

1  
2  
3  
4  
5  
6  
7  
8  
9  
10  
11  
12  
13  
14  
15  
16  
17  
18  
19  
20  
21  
22  
23  
24  
25  
26  
27  
28  
29  
30  
31  
32  
33  
34  
35  
36  
37  
38  
39  
40  
41  
42  
43  
44  
45  
46  
47  
48  
49  
50  
51  
52  
53  
54  
55  
56  
57  
58  
59  
60

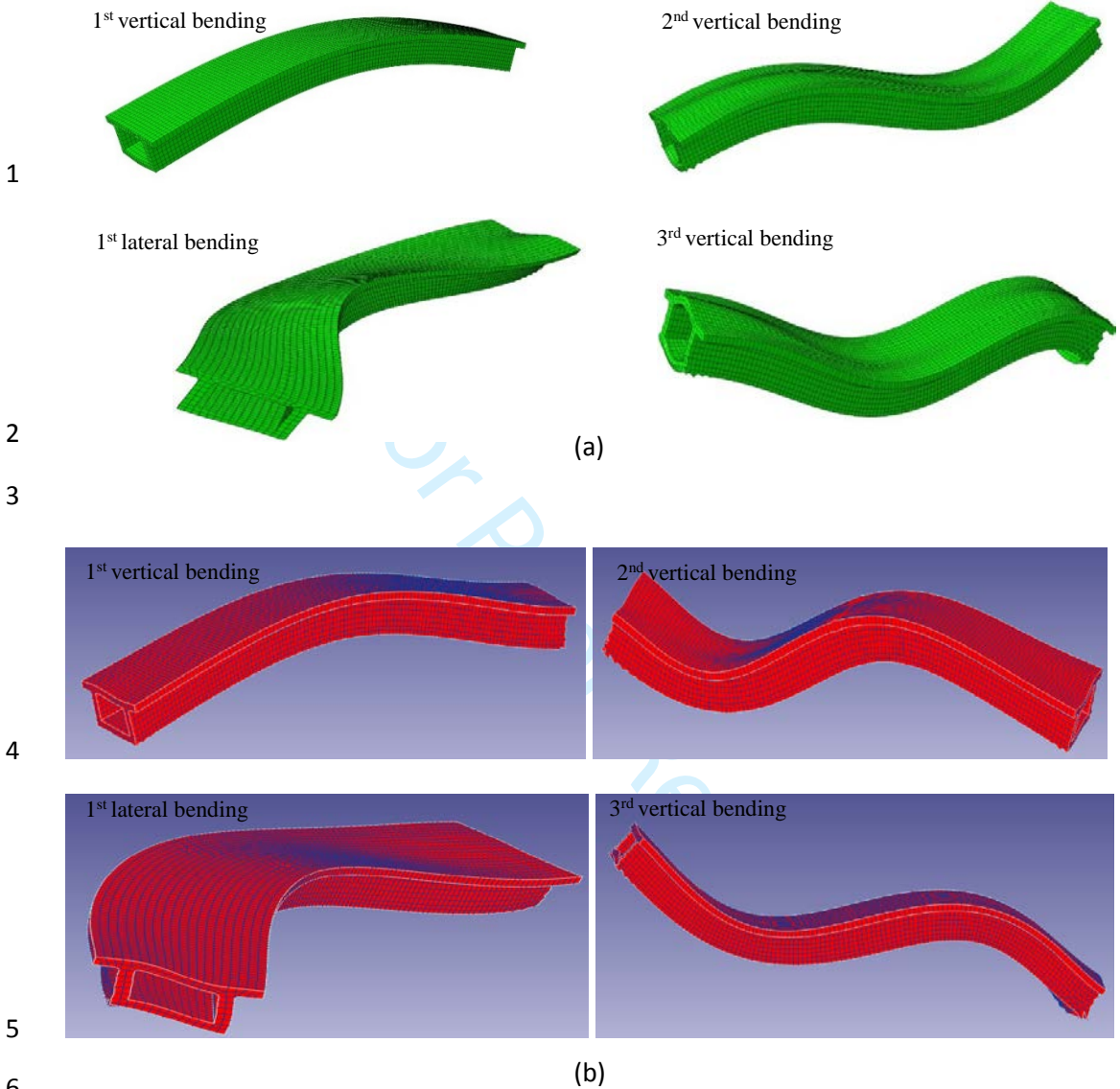


Figure 6. Four mode shapes: (a) Numerical model and (b) Measured model.

1  
2  
3  
4  
5  
6  
7  
8  
9  
10  
11  
12  
13  
14  
15  
16  
17  
18  
19  
20  
21  
22  
23  
24  
25  
26  
27  
28  
29  
30  
31  
32  
33  
34  
35  
36  
37  
38  
39  
40  
41  
42  
43  
44  
45  
46  
47  
48  
49  
50  
51  
52  
53  
54  
55  
56  
57  
58  
59  
60

## 1 *Sensitivity analysis*

2 A key step in most model updating approaches is the selection of appropriate  
3 parameters and responses in advance to initiate the updating process. Sensitivity  
4 analysis is a technique used to select the most sensitive parameters to the responses  
5 of a numerical model. This technique tends to analyse the effect of a very small  
6 perturbation of a parameter's value on a response by sketching the tangents on the  
7 response-parameter curve (Mottershead and Friswell, 2011). In this study,  
8 differential sensitivity analysis was applied to choose the most sensitive parameters  
9 to the selected responses using FEMtools (Dynamic Design Solutions, 2012). A  
10 differential sensitivity coefficient was calculated as the slope of the response  $T_i$  in  
11 relation to parameter  $B_j$  at a known state of the parameter. Once these differentials  
12 were calculated for all selected responses in relation to all selected parameters,  
13 sensitivity matrix  $\mathbf{S}$  was generated by equation (11).

$$15 \quad \mathbf{S} = S_{ij} = \frac{\delta T_i}{\delta B_j} \quad (11)$$

16 where:

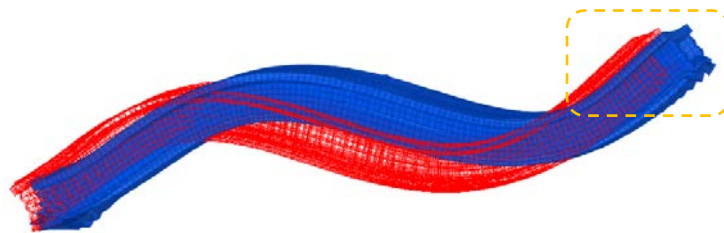
17  $i: 1, \dots, n$   $T$ : Responses

18  $j: 1, \dots, n$   $B$ : Parameters

19

1 Each column of the sensitivity matrix corresponds with a parameter  $B_j$  and each  
2 row corresponds with a response  $T_i$ . Regarding the responses in this experiment,  
3 the four modal frequencies identified in the previous subsections were selected as  
4 sensitive responses. Details of the selected responses are shown in Table 1.

5 In the initial FEM, the simple supports were modelled as fixed in the vertical  
6 direction. However, by applying a correlation analysis between the mode shapes  
7 from the FEM and those from the experiment, it was observed that the roller in the  
8 experimental model was not fixed, as a bouncing was observed in the second  
9 vertical mode shape, as shown in Figure 7. Further, similar results were obtained  
10 for the third vertical bending mode shape. Therefore, a more accurate simulation of  
11 the boundary condition was used in this study to better represent the behavior of  
12 the structure.



13  
14 **Figure 7.** Correlation between FEM (Blue) and experimental (Red) in 2<sup>nd</sup> vertical mode shape.

1  
2  
3  
4  
5  
6  
7  
8  
9 1 For the updating process, the parameters related to concrete in three different parts  
10  
11 2 (i.e., bottom slab, webs, and top slab) were selected separately because the BGB  
12  
13 3 was cast in the three corresponding steps. Further, observed changes in the health  
14  
15 4 condition of the three parts were different after the damage was induced. Hence,  
16  
17 5 the parameter selection resulted in 10 parameters: (1) Young's modulus of concrete  
18  
19 6 (top), (2) Young's modulus of concrete (web), (3) Young's modulus of concrete  
20  
21 7 (bottom), (4) Young's modulus of reinforcement, (5) vertical spring stiffness  
22  
23 8 (roller), (6) vertical spring stiffness (pinned), (7) mass density of reinforcement, (8)  
24  
25 9 mass density of concrete (top), (9) mass density of concrete (web), and (10) mass  
26  
27 10 density of concrete (bottom). Results of the sensitivity analysis, as shown in Figure  
28  
29 11 8, provide a clearer picture of which parameters were sensitive to the selected  
30  
31 12 responses. The vertical axis in this figure refers to sensitivity magnitude. Based on  
32  
33 13 the sensitivity analysis, the selection resulted in the five most sensitive parameters:  
34  
35 14 Young's moduli of the bottom slab, the webs, and the top slab ( $E_{cBot}$ ,  $E_{cWeb}$ , and  
36  
37 15  $E_{cTop}$ ); and vertical spring stiffness coefficients of the two supports ( $K_{roller}$  and  $K_{pin}$ ).  
38  
39 16 Reducing the number of parameters of interest is essential to decrease the  
40  
41 17 computational cost.  
42  
43  
44  
45  
46  
47  
48  
49  
50  
51  
52  
53  
54  
55  
56  
57  
58  
59  
60

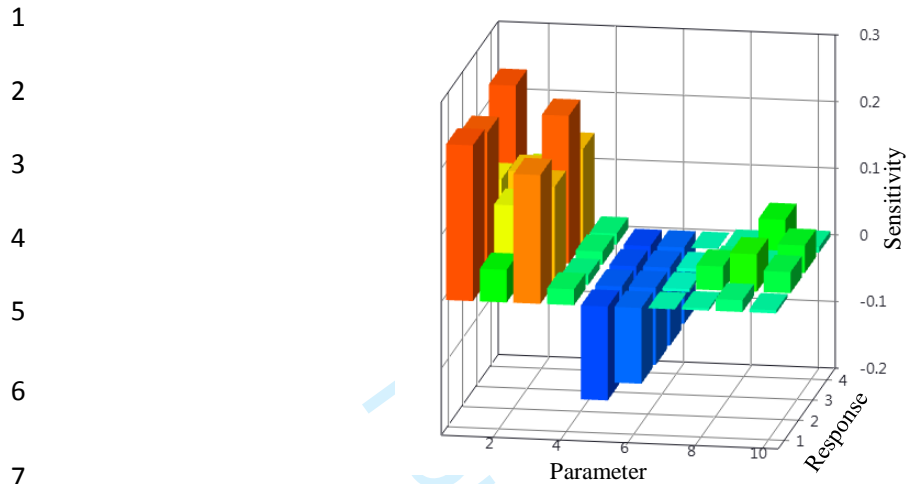


Figure 8. Sensitivity Analysis between selected parameters and responses.

## Result and discussion

The FEM of the BGB was updated for the two states—undamaged and damaged—by applying the MBA and using the four natural frequencies, mentioned in the previous section, as the responses. This section highlights the outcomes regarding the calibrated parameters and predicted responses in both states.

### *FEMU for undamaged state*

There was a lack of testing results from the casting stage, such as core sampling and tensile strength, to provide insights into prior distribution. Therefore, normal distributions were selected to represent all parameters' prior probability distribution

1 functions. This was in line with Mirza et al. (1980), Darmawan and Stewart (2007)  
 2 and recommendations from the code of practice AS-5104, as shown in Table 2.

3  
 4 **Table 2.** Parameter Prior Probability Distribution in Undamaged state

Parameter	Mean	Coefficient of Variation
( $E_{cTop}$ ) Young's modulus - Concrete - Top slab	32 GPa	7.13
( $E_{cWeb}$ ) Young's modulus - Concrete - Web	32 GPa	7.13
( $E_{cBot}$ ) Young's modulus - Concrete - Bottom slab	32 GPa	7.13
( $K_{Roller}$ ) Spring Stiffness Roller support	$5 \times 10^7$ N/m	$9 \times 10^{13}$
( $K_{Pin}$ ) Spring Stiffness Pinned support	$5 \times 10^7$ N/m	$9 \times 10^{13}$

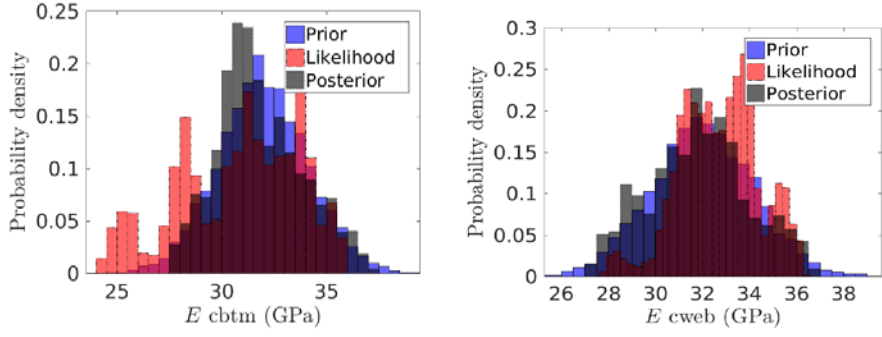
5  
 6 In this study, the computational process was carried out using a computer equipped  
 7 with an Intel i7 quad-core processor with 3.4 GHz speed, 16 GB of RAM, and a  
 8 fast-access solid-state drive (SSD). For modules 1 and 2, hyperparameters were  
 9 obtained that characterize the estimation of the calibrated parameters and the  
 10 discrepancy function, and consequently represent the GPs. These hyperparameters  
 11 included a variance matrix  $\Sigma$ , a matrix of regression coefficient  $\beta$ , roughness  
 12 parameters  $\omega$ , and a noise variance matrix  $\Lambda$ , as explained in the methodology.  
 13 Results of the calibrated parameters after applying the MBA in the undamaged state  
 14 are illustrated in Figure 9 and Table 3. The posterior may require more data before  
 15 it faithfully represents the calibrated parameters; as a result, it did not present any

1 changes compared with the prior. It is worth noting that the likelihood identified  
2 the calibrated parameters according to the measured data. As shown in Figure 9, in  
3 the undamaged state, there were no considerable changes in Young's moduli of the  
4 webs and the top slab in the likelihood against their priors. A significant change  
5 was observed in the reduction in the bottom slab's Young's modulus ( $E_{cBot}$ ), which  
6 was identical to the observed minor cracks beneath the BGB. Another noticeable  
7 change was a reduction in vertical spring stiffness at the roller support, which infers  
8 that the vertical fixity at the roller support was overestimated. This outcome is well  
9 matched with the observed bouncing in the roller previously noticed in Figure 7.

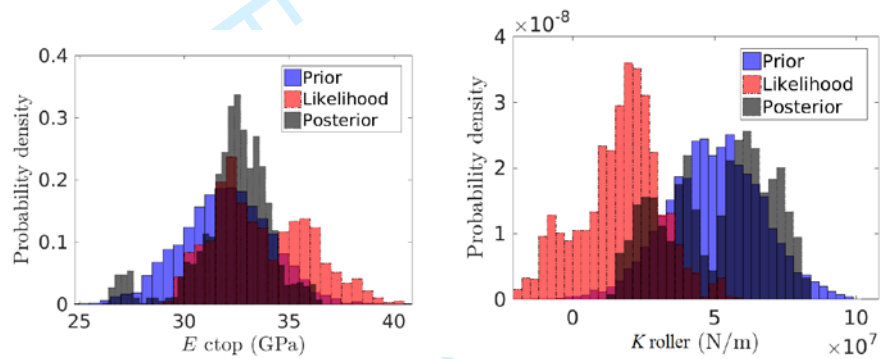
10

1  
2  
3  
4  
5  
6  
7  
8  
9  
10  
11  
12  
13  
14  
15  
16  
17  
18  
19  
20  
21  
22  
23  
24  
25  
26  
27  
28  
29  
30  
31  
32  
33  
34  
35  
36  
37  
38  
39  
40  
41  
42  
43  
44  
45  
46  
47  
48  
49  
50  
51  
52  
53  
54  
55  
56  
57  
58  
59  
60

1



2



3

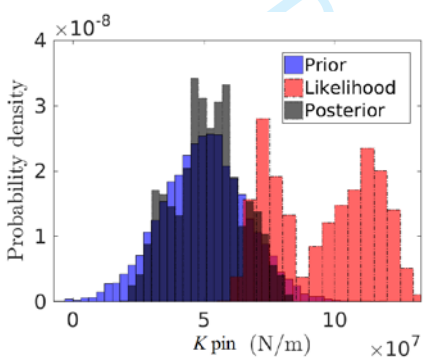


Figure 9. Prior, Max Likelihood and Posterior PDF for calibrated parameters in undamaged state.

4

5

6

**Table 3.** The Likelihood and Posterior distribution for calibrated parameters in undamaged state

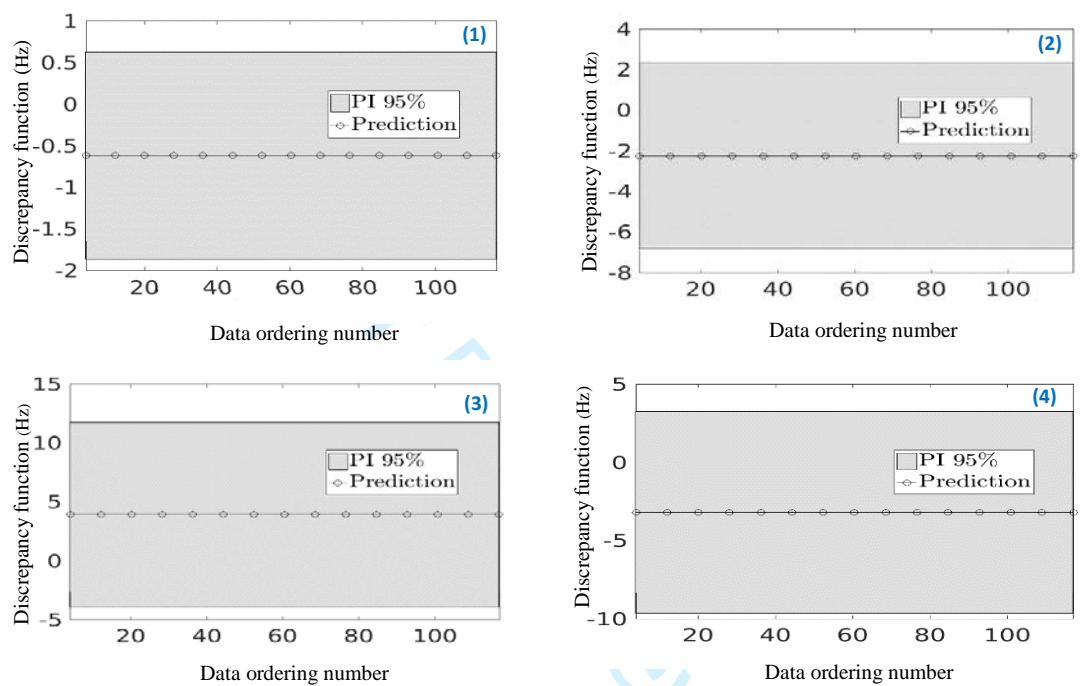
Part	Posterior		Likelihood	
	Mean	Coefficient of Variation	Mean	Coefficient of Variation
$E_{cBot}$	31.81 (GPa)	4.1	30.84 (GPa)	8.3
$E_{cWeb}$	31.83 (GPa)	4.5	32.69 (GPa)	2.9
$E_{cTop}$	32.34 (GPa)	3.4	33.67 (GPa)	5.2
$K_{Roller}$	$5.10 \times 10^7$ (N/m)	$3.32 \times 10^{14}$	$1.68 \times 10^7$ (N/m)	$2.02 \times 10^{14}$
$K_{Pin}$	$5.15 \times 10^7$ (N/m)	$1.66 \times 10^{14}$	$9.53 \times 10^7$ (N/m)	$3.82 \times 10^{14}$

The discrepancy functions for all four modes in the undamaged state are depicted in Figure 10 (a). In this figure, the horizontal axis represents the sample ordering numbers of the simulated data. The black line represents the predicted mean, and the shaded region denotes a 95% prediction interval. As shown, the MBA predicted the measured responses accurately for all modes, with deviations of less than 6%.

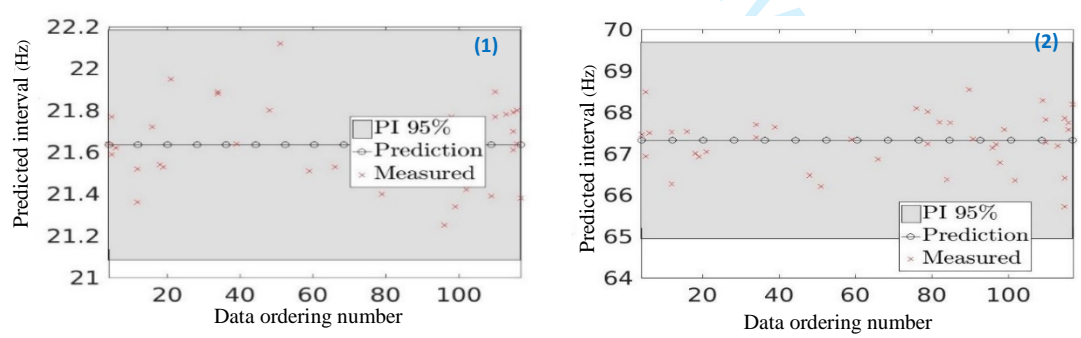
Figure 10 (b) depicts the measured responses together with the prediction intervals for all four modal frequencies. The measured data points obtained from the experimental tests, as shown by red spots in Figure 10 (b), are randomly distributed among the simulated data points. As shown, the measured data points are located in the 95% prediction interval and are very close to the mean values of the predicted responses. The predicted mean values almost coincide with those of the measured data points for all modes (see Table 1). However, it can be inferred from the

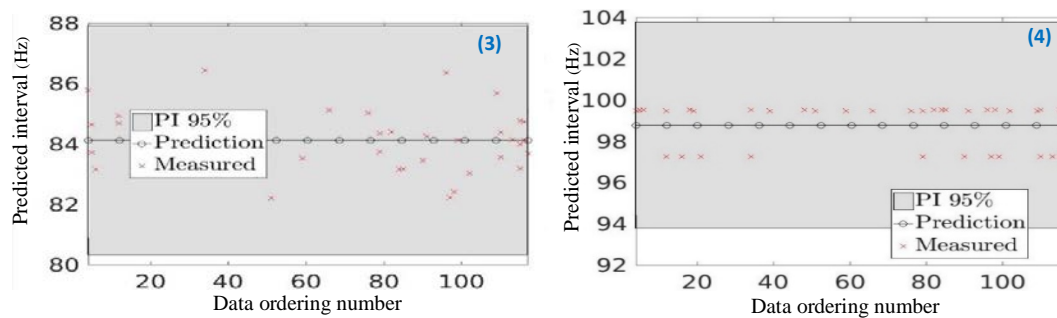
1  
2  
3  
4  
5  
6  
7  
8  
9  
10  
11  
12  
13  
14  
15  
16  
17  
18  
19  
20  
21  
22  
23  
24  
25  
26  
27  
28  
29  
30  
31  
32  
33  
34  
35  
36  
37  
38  
39  
40  
41  
42  
43  
44  
45  
46  
47  
48  
49  
50  
51  
52  
53  
54  
55  
56  
57  
58  
59  
60

- 1 predictions that the higher the mode order that is examined, the larger the scatter
- 2 interval that is obtained.



(a) Discrepancy functions for frequency responses.





(b) Predicted interval 95% confidence for numerical model and experimental data points.

**Figure 10.** The results of Discrepancy function and predicted response for numerical model in undamaged state for all four modal frequencies as: (1) 1<sup>st</sup> vertical bending frequency, (2) 2<sup>nd</sup> vertical bending frequency, (3) 1<sup>st</sup> lateral bending frequency & (4) 3<sup>rd</sup> vertical bending frequency.

### *FEMU for damaged state*

The next step of model updating refers to the damaged state, where some significant cracks were observed on the bottom slab and the webs of the BGB. It is worth mentioning that the number of calibrated parameters was reduced to three (Young's moduli) because it was assumed that the applying impacts in the damaged state did not affect the boundary conditions. Results of the prior, likelihood, and posterior distributions of the calibrated parameters are illustrated in Figure 11 and Table 4.

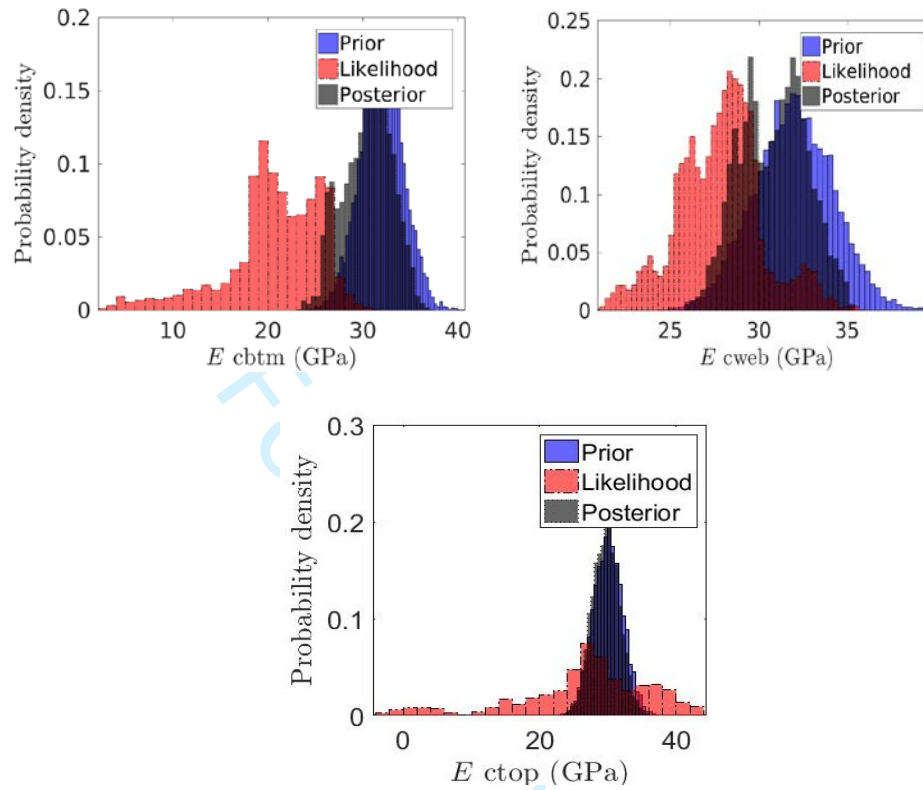


**Figure 11.** Prior, Max Likelihood and Posterior PDF for calibrated parameters in damaged state.

**Table 4.** The Likelihood and Posterior distribution for calibrated parameters in damaged state

Part	Posterior		Likelihood	
	mean	Coefficient of Variation	mean	Coefficient of Variation
$E_{cBot}$	30.45 (GPa)	6.45	20.63 (GPa)	25.59
$E_{cWeb}$	30.82 (GPa)	3.58	27.82 (GPa)	5.99
$E_{cTop}$	32.54 (GPa)	2.26	30.54 (GPa)	35.45

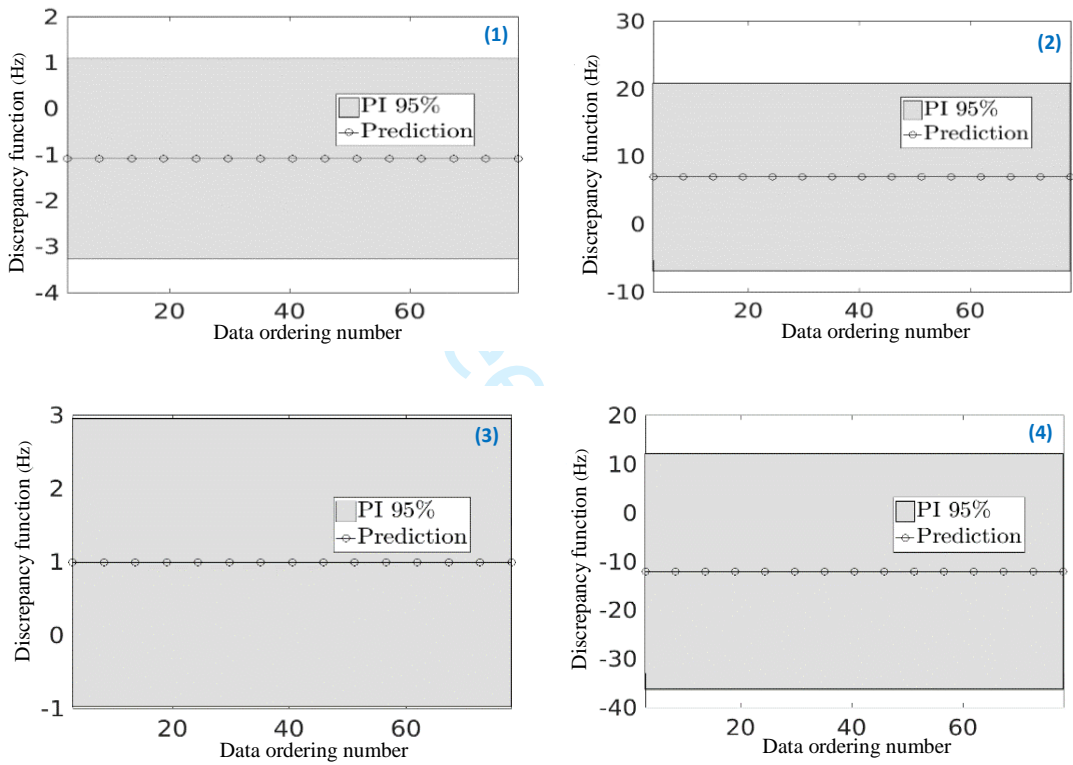
1  
2  
3  
4  
5  
6  
7  
8  
9 1 As shown in Figure 11, a significant change was targeted at the likelihood in  
10  
11 2 Young's modulus of the bottom slab, indicating a reduction of about 35.5% to a  
12  
13 3 new mean value of 20.63 GPa. Further, the decrease in Young's modulus of the  
14  
15 4 web section was noticeable, showing a likelihood mean of 27 GPa. The impact  
16  
17 5 forces had little effect on the top slab, and its updated Young's modulus was almost  
18  
19 6 the same as its initial value. The reduction in the Young's moduli of the bottom  
20  
21 7 slab and the webs is well matched with the cracks observed in the damaged state,  
22  
23 8 as mentioned in the section *Two states of box girder bridge*. The discrepancy  
24  
25 9 functions for all four modes in the damaged state are depicted in Figure 12 (a). As  
26  
27 10 shown in the figure, the discrepancy increases in the damaged state, especially for  
28  
29 11 the second and third vertical bending modes. In addition, the discrepancy functions  
30  
31 12 in the damaged state are distributed more sparsely than those in the undamaged  
32  
33 13 state. This may be because the cracks cause nonlinearities in the properties of  
34  
35 14 structural materials and the mechanism of the experimental response.

36  
37  
38  
39  
40  
41  
42 15 Results of the measured responses together with predicted intervals for all four  
43  
44 16 modes are shown in Figure 12 (b). As shown, the measured data points are observed  
45  
46 17 in the corresponding predicted intervals and are very close to the mean values for  
47  
48 18 all modes except the last one (third vertical bending mode). Results for the third  
49  
50 19 vertical bending mode are very scattered. It is worth noting that the discrepancy of  
51  
52 20 this mode is larger than that of the other modes, as shown in Figure 12 (b). This can  
53  
54  
55  
56  
57  
58  
59  
60

1  
2  
3  
4  
5  
6  
7  
8  
9  
10  
11  
12  
13  
14  
15  
16  
17  
18  
19  
20  
21  
22  
23  
24  
25  
26  
27  
28  
29  
30  
31  
32  
33  
34  
35  
36  
37  
38  
39  
40  
41  
42  
43  
44  
45  
46  
47  
48  
49  
50  
51  
52  
53  
54  
55  
56  
57  
58  
59  
60

1 be explained because nonlinearity effects resulting from cracks become more  
2 significant when the vibration mode contains a higher-order curve.

3

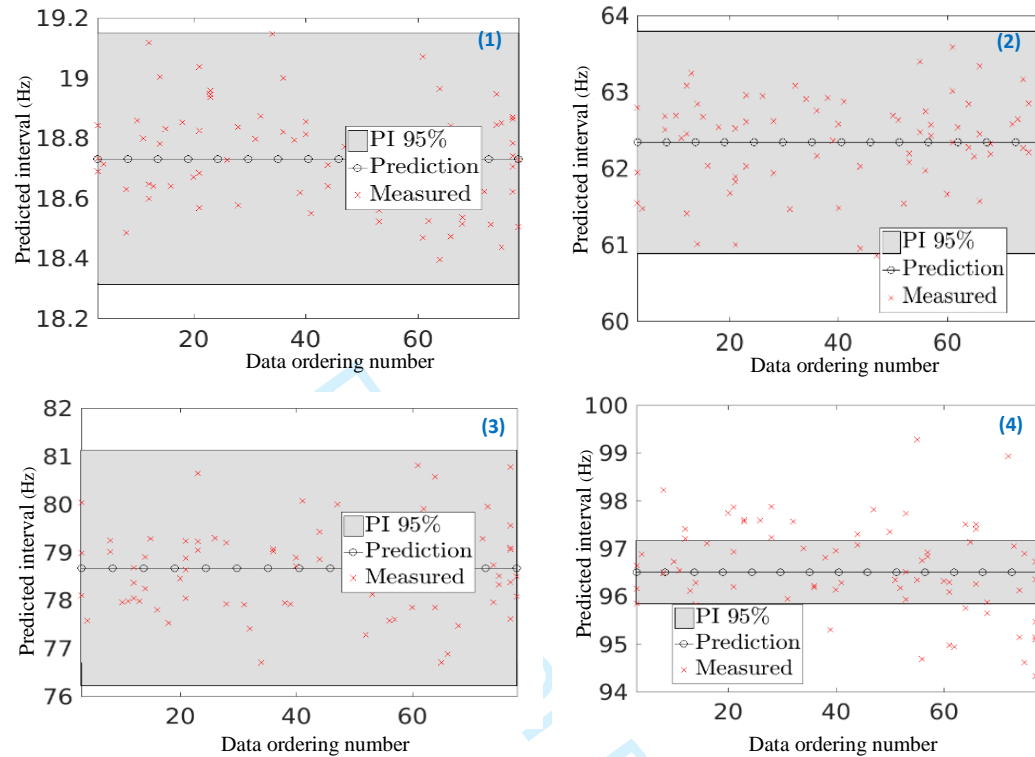


4

5

(a) Discrepancy functions for frequency responses.

6



(b) Predicted interval 95% confidence for numerical model and experimental data points.

**Figure 12.** The results of discrepancy function and predicted response for numerical model in damaged state, for all four modal frequencies as: (1) 1<sup>st</sup> vertical bending frequency, (2) 2<sup>nd</sup> vertical bending frequency, (3) 1<sup>st</sup> lateral bending frequency & (4) 3<sup>rd</sup> vertical bending frequency.

## Conclusions

In this study, the performance of an MBA was investigated in a large lab-scaled BGB using vibration data. Sensitivity analysis was conducted to select the most sensitive parameters and responses. Further, a metamodel was used instead of a

1  
2  
3  
4  
5  
6  
7  
8  
9  
10  
11  
12  
13  
14  
15  
16  
17  
18  
19  
20  
21  
22  
23  
24  
25  
26  
27  
28  
29  
30  
31  
32  
33  
34  
35  
36  
37  
38  
39  
40  
41  
42  
43  
44  
45  
46  
47  
48  
49  
50  
51  
52  
53  
54  
55  
56  
57  
58  
59  
60

1 whole numerical model. Therefore, the computational task and processing time was  
2 reduced in comparison with other probabilistic updating techniques. This benefit  
3 distinguishes this approach, especially in applications to complex structures.

4 This study is the first to apply the MBA for two different states: damaged and  
5 undamaged. These two states represent the health conditions of the structure during  
6 its life span, and the outcomes can be used for further structural investigations.

7 Although a case study is rather simple compared with full-scale real structures, such  
8 a scale provides a possibility to investigate the performance of the proposed  
9 approach in two different states according to the observed evidence on the structure.  
10 Further, this study highlighted the advantages of FEMU because it illustrated that  
11 even an FEM of a downscaled structure requires accurate calibration to be reliably  
12 used in further structural assessments.

13 Moreover, in contrast to many previous studies, which applied the MBA to a single  
14 parameter, this study investigated model updating on multiple parameters, such as  
15 material properties and boundary conditions, at the same time. In this study, the  
16 changes to these parameters were well matched with the observed evidence in both  
17 states. Natural frequencies of the first four modes, used as the measured data points,  
18 were predicted correctly. The updated model was sufficiently matched with the  
19 physical observation of the damaged structure. In turn, the results generated from

1 this study might be attributed to the proposed uncertainty quantification  
2 methodology. Further, as the results showed in the damaged state, the discrepancy  
3 functions increased, and experimental responses were not predicted as accurately  
4 as in the undamaged state. Such increases in the discrepancy functions are inferred  
5 as a guide for designers, implying that the FEM needs to be refined by considering  
6 additional aspects such as crack modeling. Further, response prediction can be  
7 improved and discrepancy can be reduced by adding other experimental data points  
8 (e.g., strain and mode shape) and information about environmental conditions (e.g.,  
9 temperature and humidity). Although natural frequency was selected as the  
10 response for the updating process in this study, the MBA is capable of considering  
11 other types of responses. Thus, the performance of the approach when applied to  
12 other responses, such as mode shape, should be investigated in future studies.  
13 Consequently, the proposed methodology contributes to more reliable judgments  
14 about structural safety and more informed maintenance decision-making.

1  
2  
3  
4  
5  
6  
7  
8  
9  
10  
11  
12  
13  
14  
15  
16  
17  
18  
19  
20  
21  
22  
23  
24  
25  
26  
27  
28  
29  
30  
31  
32  
33  
34  
35  
36  
37  
38  
39  
40  
41  
42  
43  
44  
45  
46  
47  
48  
49  
50  
51  
52  
53  
54  
55  
56  
57  
58  
59  
60

## 1 **Acknowledgments**

2 The first author would like to express his sincere appreciation to Queensland  
3 University of Technology (QUT) for the financial support for his research. The support  
4 provided by Australian Research Council (ARC) via a Discovery Project  
5 (DP160101764) is also gratefully acknowledged. Also, the support provided by  
6 technical support from FEMtools is acknowledged.

## 9 **References**

- 10 Arendt, P.D., Apley, D.W. and Chen, W (2012a) Quantification of model uncertainty:  
11 Calibration, model discrepancy, and identifiability. *Journal of Mechanical*  
12 *Design* 134(10):100908-100908-12.
- 13
- 14 Arendt, P.D., Apley, D.W., Chen, W., Lamb, D. and Gorsich, D (2012b) Improving  
15 identifiability in model calibration using multiple responses. *Journal of Mechanical*  
16 *Design* 134(10) 100909-100909-9.
- 17
- 18 Abaqus, F.E.A. (2017) Abaqus Inc. *Providence, Rhode Island, United States.*

- 1  
2  
3  
4  
5  
6  
7  
8  
9 1 Bayarri, M. J., Berger, J. O., Paulo, R., Sacks, J., Cafeo, J. A., Cavendish, J., Lin, C.  
10  
11 2 H., and Tu, J (2007) “A Framework for Validation of Computer Models,”  
12  
13 3 *Technometrics* 49(2), pp. 138–154.  
14  
15  
16 4  
17  
18 5 Beck, J.L. and Au, S.K. (2002) Bayesian updating of structural models and reliability  
19  
20 6 using Markov chain Monte Carlo simulation. *Journal of engineering*  
21  
22 7 *mechanics* 128(4), pp.380-391.  
23  
24  
25 8  
26  
27 9 Beck, J.L. and Katafygiotis, L. S (1998) Updating models and their uncertainties. I:  
28  
29 10 Bayesian statistical framework. *Journal of Engineering Mechanics* 124(4), pp.455-  
30  
31 11 461.  
32  
33  
34 12  
35  
36 13 Conde, B., Eguía, P., Stavroulakis, G.E. and Granada, E. (2018) Parameter  
37  
38 14 identification for damaged condition investigation on masonry arch bridges using a  
39  
40 15 Bayesian approach. *Engineering Structures* 172, pp.275-284.  
41  
42  
43 16  
44  
45 17 Conti, S., Gosling, J.P., Oakley, J.E. and O'Hagan, A. (2009) Gaussian process  
46  
47 18 emulation of dynamic computer codes. *Biometrika* 96(3), pp.663-676.  
48  
49  
50 19  
51  
52  
53  
54  
55  
56  
57  
58  
59  
60

1  
2  
3  
4  
5  
6  
7  
8  
9  
10  
11  
12  
13  
14  
15  
16  
17  
18  
19  
20  
21  
22  
23  
24  
25  
26  
27  
28  
29  
30  
31  
32  
33  
34  
35  
36  
37  
38  
39  
40  
41  
42  
43  
44  
45  
46  
47  
48  
49  
50  
51  
52  
53  
54  
55  
56  
57  
58  
59  
60

1 Darmawan, M.S. and Stewart, M.G. (2007) Spatial time-dependent reliability analysis  
2 of corroding pretensioned prestressed concrete bridge girders. *Structural Safety* 29(1),  
3 pp.16-31.

4  
5 FEMtools UM (2012) *FEMtools Dynamic Design Solutions* N.V. (DDS)

6  
7 Frangopol, D.M. (2011) Life-cycle performance, management, and optimisation of  
8 structural systems under uncertainty: accomplishments and challenges 1. *Structure*  
9 *and Infrastructure Engineering* 7(6), pp.389-413.

10  
11 Friswell, M. and Mottershead, J.E. (2013) Finite element model updating in structural  
12 dynamics (Vol. 38). Springer Science & Business Media.

13  
14 General principles on reliability for structures (AS 5104)

15  
16 Higdon, D., Gattiker, J., Williams, B. and Rightley, M. (2008) Computer model  
17 calibration using high-dimensional output. *Journal of the American Statistical*  
18 *Association* 103(482), pp.570-583.

19

- 1  
2  
3  
4  
5  
6  
7  
8  
9 1 Jamali, S., Chan, T.H., Nguyen, A. and Thambiratnam, D.P. (2018) Reliability-based  
10  
11 2 load-carrying capacity assessment of bridges using structural health monitoring and  
12  
13 3 nonlinear analysis. *Structural Health Monitoring* 18(1), pp. 20–34.  
14  
15  
16 4  
17  
18 5 Jamali, S., Chan, T.H., Thambiratnam, D.P., Pritchard, R. and Nguyen, A. (2016) Pre-  
19  
20 6 test finite element modelling of box girder overpass-application for bridge condition  
21  
22 7 assessment. In *Australasian Structural Engineering Conference: ASEC 2016* (p. 457).  
23  
24 8 Engineers Australia.  
25  
26  
27 9  
28  
29 10 Jesus, A., Brommer, P., Westgate, R., Koo, K., Brownjohn, J. and Laory, I. (2018)  
30  
31 11 Bayesian structural identification of a long suspension bridge considering temperature  
32  
33 12 and traffic load effects. *Structural Health Monitoring*  
34  
35 13 <https://doi.org/10.1177/1475921718794299>  
36  
37 14  
38  
39 15 Jesus, A., Brommer, P., Westgate, R., Koo, K., Brownjohn, J., & Laory, I. (2019)  
40  
41 16 Modular Bayesian damage detection for complex civil infrastructure. *Journal of Civil*  
42  
43 17 *Structural Health Monitoring* 1-15.  
44  
45  
46  
47  
48  
49  
50  
51  
52  
53  
54  
55  
56  
57  
58  
59  
60

1  
2  
3  
4  
5  
6  
7  
8  
9  
10  
11  
12  
13  
14  
15  
16  
17  
18  
19  
20  
21  
22  
23  
24  
25  
26  
27  
28  
29  
30  
31  
32  
33  
34  
35  
36  
37  
38  
39  
40  
41  
42  
43  
44  
45  
46  
47  
48  
49  
50  
51  
52  
53  
54  
55  
56  
57  
58  
59  
60

- 1 Jesus, A., Brommer, P., Zhu, Y. and Laory, I. (2017) Comprehensive Bayesian  
2 structural identification using temperature variation. *Engineering Structures* 141,  
3 pp.75-82.
- 4
- 5 Jesus, A.H., Dimitrovová, Z. and Silva, M.A. (2014) A statistical analysis of the  
6 dynamic response of a railway viaduct. *Engineering Structures* 71, pp.244-259.
- 7
- 8 Kennedy, M. and O'Hagan, A. (2001a) Bayesian calibration of computer  
9 models. *Journal of the Royal Statistical Society: Series B (Statistical*  
10 *Methodology)* 63(3), pp.425-464.
- 11
- 12 Kennedy, M. and O'Hagan, A. (2001b). Supplementary details on Bayesian calibration  
13 of computer. Rap. tech., University of Nottingham *Statistics Section*.
- 14
- 15 Li, H.N., Li, D.S., Ren, L., Yi, T.H., Jia, Z.G. and Li, K.P. (2016) Structural health  
16 monitoring of innovative civil engineering structures in Mainland China. *Structural*  
17 *Monitoring and Maintenance* 3(1), pp.1-32.
- 18
- 19 Liu, F., Bayarri, M.J. and Berger, J.O. (2009) Modularization in Bayesian analysis,  
20 with emphasis on analysis of computer models. *Bayesian Analysis* 4(1), pp.119-150.

- 1  
2  
3  
4  
5  
6  
7  
8  
9 1 Lophaven, S.N., Nielsen, H.B. and Søndergaard, J. (2002) *DACE: a Matlab kriging*  
10  
11 2 *toolbox* (Vol. 2). IMM, *Informatics and Mathematical Modelling, the Technical*  
12  
13 3 *University of Denmark.*  
14  
15  
16 4  
17  
18 5 Mirza, S.A., Kikuchi, D.K. and MacGregor, J.G. (1980) Flexural strength reduction  
19  
20 6 factor for bonded prestressed concrete beams. In *Journal Proceedings* (Vol. 77, No. 4,  
21  
22 7 pp. 237-246).  
23  
24  
25 8  
26  
27 9 Moravej H, Jamali S, Chan THT, Nguyen A. (2017) Finite element model updating of  
28  
29 10 civil engineering infrastructures: a review literature. *International Conference on*  
30  
31 11 *Structural Health Monitoring of Intelligent Infrastructure. Brisbane, Australia 2017.*  
32  
33  
34 12  
35  
36 13 Mottershead, J.E., Link, M. and Friswell, M.I. (2011) The sensitivity method in finite  
37  
38 14 element model updating: a tutorial. *Mechanical systems and signal processing* 25(7),  
39  
40 15 pp.2275-2296.  
41  
42  
43 16  
44  
45 17 O'Hagan, A. (2006) Bayesian analysis of computer code outputs: A  
46  
47 18 tutorial. *Reliability Engineering & System Safety* 91(10-11), pp.1290-1300.  
48  
49  
50 19  
51  
52  
53  
54  
55  
56  
57  
58  
59  
60

1  
2  
3  
4  
5  
6  
7  
8  
9  
10  
11  
12  
13  
14  
15  
16  
17  
18  
19  
20  
21  
22  
23  
24  
25  
26  
27  
28  
29  
30  
31  
32  
33  
34  
35  
36  
37  
38  
39  
40  
41  
42  
43  
44  
45  
46  
47  
48  
49  
50  
51  
52  
53  
54  
55  
56  
57  
58  
59  
60

- 1 Pathirage TS. (2017). Identification of prestress force in prestressed concrete box  
2 girder bridges using vibration-based techniques. *Queensland University of*  
3 *Technology*.
- 4
- 5 Rasmussen, C. and Williams, C. (2006) Gaussian Processes for Machine Learning.  
6 *Adaptive Computation and Machine Learning*.
- 7
- 8 Shahidi, S.G. and Pakzad, S.N. (2013) Generalized response surface model updating  
9 using time domain data. *Journal of Structural Engineering* 140(8), p.A4014001.
- 10
- 11 Simoen, E., Papadimitriou, C. and Lombaert, G. (2013) On prediction error correlation  
12 in Bayesian model updating. *Journal of Sound and Vibration* 332(18), pp.4136-4152  
13
- 14 Structural Vibration Solutions A/S (2011) SVS-ARTEMIS Extractor-Release 5.3,  
15 User's manual. Aalborg-Denmark
- 16
- 17 Weng, S., Xia, Y., Zhou, X.Q., Xu, Y.L. and Zhu, H.P. (2012) Inverse substructure  
18 method for model updating of structures. *Journal of Sound and Vibration* 331(25),  
19 pp.5449-5468.